Geodynamic Significance of Seismic Anisotropy of the Upper Mantle: New Insights from Laboratory Studies

Shun-ichiro Karato,[1] Haemyeong Jung,[2] Ikuo Katayama,[3] and Philip Skemer[1]

[1]Department of Geology & Geophysics, Yale University, New Haven, Connecticut 06511; email: shun-ichiro.karato@yale.edu

[2]School of Earth and Environmental Sciences, Seoul National University, Seoul 151-747, South Korea

[3]Department of Earth and Planetary Sciences, Hiroshima University, Higashi Hiroshima 739-8526, Japan

Annu. Rev. Earth Planet. Sci. 2008. 36:59–95

First published online as a Review in Advance on November 20, 2007

The *Annual Review of Earth and Planetary Sciences* is online at earth.annualreviews.org

This article's doi:
10.1146/annurev.earth.36.031207.124120

0084-6597/08/0530-0059$20.00

Key Words

lattice-preferred orientation, olivine, water, partial melting, seismic anisotropy

Abstract

Seismic anisotropy is caused mainly by the lattice-preferred orientation of anisotropic minerals. Major breakthroughs have occurred in the study of lattice-preferred orientation in olivine during the past ~10 years through large-strain, shear deformation experiments at high pressures. The role of water as well as stress, temperature, pressure, and partial melting has been addressed. The influence of water is large, and new results require major modifications to the geodynamic interpretation of seismic anisotropy in tectonically active regions such as subduction zones, asthenosphere, and plumes. The main effect of partial melting on deformation fabrics is through the redistribution of water, not through a change in deformation geometry. A combination of new experimental results with seismological observations provides new insights into the distribution of water associated with plume-asthenosphere interactions, formation of the oceanic lithosphere, and subduction. However, large uncertainties remain regarding the role of pressure and the deformation fabrics at low stress conditions.

INTRODUCTION

LPO: lattice-preferred orientation

V_{SH}: velocity of horizontally polarized shear waves

V_{SV}: velocity of vertically polarized shear waves

Plastic deformation of rocks often results in anisotropic structures. Anisotropic structures can be investigated directly from naturally deformed rock samples to infer deformation conditions in Earth's crust and upper mantle. Anisotropic structures in Earth's interior can also be inferred from geophysical observations such as seismic anisotropy, which can provide important constraints on the nature of deformation in Earth's interior. Anisotropic structures caused by the nonrandom distribution of crystallographic orientations of minerals (lattice-preferred orientation, LPO) have attracted much attention in earth science because the basic principles for the development of LPO are well understood, and therefore the inference of deformation conditions from these anisotropic structures can be made on a solid basis, and because anisotropy due to LPO is large and can be detected by seismology. In the early 1970s, classical experimental studies were conducted to determine the relationship between LPO and deformation conditions for olivine and other minerals (Carter & Avé Lallemant 1970, Nicolas et al. 1973). Zhang & Karato (1995) extended these earlier studies on olivine to simple shear geometry. These results formed a basis for the inference of deformation geometry of Earth's upper mantle from seismic anisotropy. These studies showed that after large-strain deformation the olivine [100] axes are oriented nearly parallel to the flow direction, and the olivine (010) planes become nearly parallel to the flow plane, which leads to (*a*) $\frac{V_{SH}}{V_{SV}} > 1$ for horizontal flow and to $\frac{V_{SH}}{V_{SV}} < 1$ for vertical flow, and (*b*) the direction of polarization of the faster shear wave to become parallel to the flow direction. This notion has been the paradigm in the geodynamic interpretation of upper mantle anisotropy for almost 30 years (e.g., Montagner & Guillot 2002, Nicolas & Christensen 1987, Park & Levin 2002, Savage 1999).

However, new findings during the past ~10 years suggest that this paradigm may need drastic modifications when applied to some geologically important regions. Using high-pressure simple shear deformation techniques developed by Karato & Rubie (1997) and Zhang & Karato (1995), a number of new experimental studies have been conducted on the development of olivine LPO. First, a series of experimental studies in our laboratory showed that olivine LPO is sensitive to water content as well as stress and temperature (e.g., Jung & Karato 2001, Jung et al. 2006, Katayama et al. 2004, Katayama & Karato 2006). Second, Couvy et al. (2004) reported that olivine LPO at high pressures is different from that at lower pressures, and they proposed that pressure might change olivine LPO (see also Raterron et al. 2007, Mainprice et al. 2005). Third, Holtzman et al. (2003) found that when partial melting occurs and deformation is localized in the melt-rich bands, the olivine LPO developed in their experimental studies is different from that developed in melt-free samples, suggesting that the deformation geometry of the solid part of a partially molten material could be different from the macroscopic deformation geometry. Holtzman et al. (2003) discussed that such a difference occurs also in natural settings and argued that the relation between LPO and the geometry of bulk flow will be different in regions of partial melting and in melt-free regions.

If true, these observations would imply that the paradigm of the relation between seismic anisotropy and deformation geometry will need major modifications, and

that in some cases the direction of the fast shear wave polarization is normal to the flow direction and that $\frac{V_{SH}}{V_{SV}} < 1$ could correspond to horizontal flow. However, the interpretation of these new experimental results is not straightforward, and as we show in this review, some of the published interpretations are likely not appropriate. The main objective of this review is to provide a critical assessment of these new results on olivine[1] to help the reader understand the current status of research on this topic.

We first review the basic physics of LPO development followed by a brief historical review of experimental studies on olivine LPO. Theoretical models for fabric transitions are also discussed. Following the review of the materials science aspects of LPO, geological and geophysical observations pertinent to olivine LPO are summarized. Finally, we summarize the present status of studies on LPO in olivine and other upper mantle minerals and discuss some future directions.

FUNDAMENTALS OF DEFORMATION FABRICS

Physical Principles of LPO Development

The mechanisms of LPO development have been reviewed in several places (e.g., Wenk 1985; Karato 2008, chapter 14), and therefore only their essence is summarized here. LPO develops by deformation due to dislocation glide (or twinning) or by recrystallization. In many cases the influence of dislocation glide is dominant, and therefore we consider LPO development by dislocation glide.

Deformation by dislocation glide (slip)[2] is simple shear and hence has a rigid body rotation component. The lattice rotation relative to the external reference frame occurs because of a mismatch between the rotational component of deformation of a crystal and the imposed macroscopic deformation. As a result, a crystal will rotate with a specific trajectory that depends on the orientation of the crystal. The velocity of rotation of crystallographic axes depends on the orientation of a crystal relative to the external framework, which leads to the development of LPO. Therefore LPO developed by this mechanism is essentially controlled by the geometry of deformation rather than the orientation of stress.

Because many slip systems are involved in the deformation of a polycrystalline aggregate, the details of LPO development can be complicated. However, when subsidiary mechanisms contribute significantly to total strain, then deformation by a single slip system can accommodate most of strain and hence will dominate LPO development. The relatively simple correlation observed between LPO and the relative easiness of the slip systems in olivine suggests that for olivine, this simplifying view (single slip LPO) is a good approximation. There are two reasons for this. First, in olivine (and in most other minerals), the strain rate due to dislocation creep is not far

[1]A short note will be provided, for completeness, on LPO of orthopyroxene and other secondary minerals, but the experimental studies on LPO in these minerals is much less extensive than those on olivine.

[2]A slip system is defined by the slip direction (Burgers vector, **b**) and the slip plane (defined by its normal vector, **n**).

from strain rate due to diffusion creep at typical geological conditions (e.g., Karato 1998, Karato et al. 1986), and therefore the strain accommodation is taken care of by diffusion creep (or grain-boundary sliding), allowing a polycrystalline material to deform using mainly the softest slip system. Second, in many cases, deformation by the softest slip system is much easier than deformation by the other slip systems. If these conditions are met, a single slip LPO model provides a reasonable description of the nature of LPO.

In cases in which a single slip system dominates, the orientation of grains with the lowest rotational velocity is the one for which the microscopic shear by dislocation glide agrees with the imposed shear. For those grains, microscopic and macroscopic shear agree and hence there is little misfit to cause rotation of a crystal. As a result, for those minerals, the relation between LPO and the slip systems is simple: In simple shear, LPO is such that grains tend to become oriented toward the direction in which microscopic shear due to dislocation glide agrees with the imposed macroscopic shear. Both olivine and orthopyroxene belong to this class of mineral. We use this simple model in most of the discussion that follows, although some exceptions are noted.

Given this single slip model, the relation between flow geometry and crystalline slip is simple. In simple shear deformation, such as the deformation of materials beneath the lithosphere, the slip plane is parallel to the macroscopic flow plane and slip direction is parallel to the macroscopic flow direction (**Figure 1**, left panel). In plume-like cylindrical flow, the slip direction of a crystal becomes parallel to the flow direction (**Figure 1**, right panel). When a large number of waves horizontally propagating (surface waves) along many directions are used, an assumption of transverse isotropy

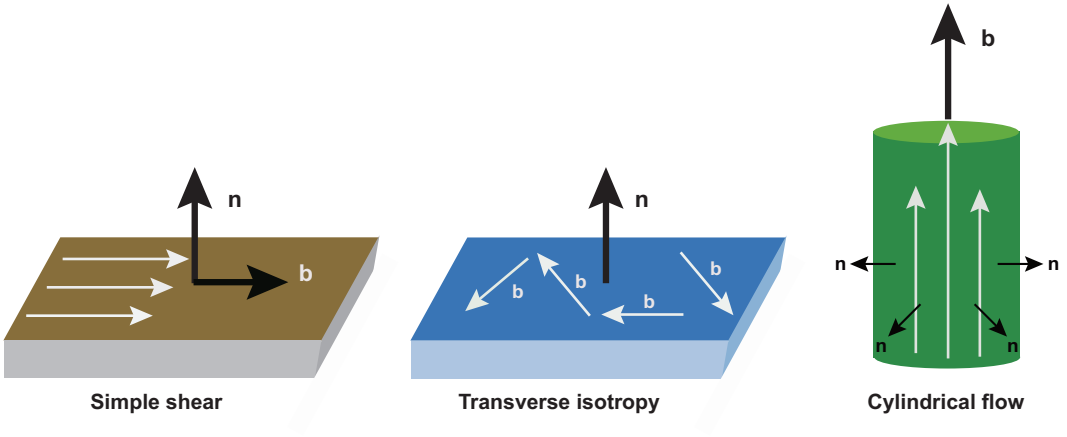

Figure 1

Diagrams showing the relation between the dominant slip system (slip direction **b**, slip plane normal **n**) and the geometry of anisotropic structure. Deformation of materials near the moving lithosphere is nearly simple shear. Transverse isotropy is assumed in some global inversion of surface wave data that involve a large number of waves propagating along many different directions. Cylindrical flow is a good approximation for a plume.

is often made in which properties are assumed to be independent of directions in a symmetry plane (**Figure 1**, middle panel).

Slip Systems

Given this simple model, the easiest or softest slip system is the characteristic that determines which LPO is likely to predominate. In a given crystal, one can imagine a variety of slip systems, and deformation is achieved by contributions from each of these slip systems. Among the two directions that characterize a slip system (slip direction and slip plane normal), the slip direction is primarily controlled by the length of the Burgers vector, with the shortest one favored because of the lower strain energy associated with dislocation formation/motion. In olivine either $\mathbf{b} = [100]$ (0.476 nm at ambient condition) or $\mathbf{b} = [001]$ (0.598 nm) is preferred (the length of $\mathbf{b} = [010]$ is 1.02 nm and hence slip along this direction is not favored). However, the difference in the length of these two Burgers vectors is small, and consequently a change in physical/chemical environment could change the dominant slip direction.[3] The choice of the slip plane is determined by more subtle factors. The magnitude of the Peierls stress (resistance to shear at $T = 0$ K) provides some guidance for the choice of a glide plane. For a given Burgers vector, the favored slip plane is the one for which h/b (h is the distance between slip planes, b is the length of the Burgers vector) is the largest (anisotropy in elastic constants is also important but this crystallographic factor often dominates). However, the relative easiness of various slip systems at high temperature depends on the relative strain rates for each slip system, which depends only indirectly on the Peierls stress. For example, in materials with relatively strong chemical bonds and a large unit cell, deformation is often controlled by dislocation glide. In this case, the rate of deformation is controlled by the concentration (and mobility) of kinks on a dislocation line, which are in turn determined by the kink nucleation energy, which is dependent on the Peierls stress. When a kink is hydrated, the Peierls stress is likely reduced, and kink concentration will increase (e.g., Heggie & Jones 1986) and the rate of deformation due to that slip system will be enhanced. I. Katayama & S.-I. Karato (manuscript submitted, 2007) reported evidence for the reduction of the Peierls stress in olivine by hydration. However, the dominant slip system may also be controlled by other factors such as the anisotropy of diffusion-controlled dislocation climb.

Physical Mechanisms of Fabric Transitions

For a given material, several different LPOs can be developed depending on the physical and chemical conditions of deformation. Several processes generate LPO, each of which develops LPO at some characteristic rate. Under a given condition, one process operates faster than others and if these processes are independent, the fastest

[3] In contrast, for orthopyroxene, the unit cell dimension is [100] = 1.82 nm, [010] = 0.881 nm, and [001] = 0.518 nm and consequently, $\mathbf{b} = [001]$ is strongly favored in comparison to other slip directions.

process will determine the type of LPO that is formed. Therefore, a fabric transition will occur when the kinetics of a process causing one type of fabric becomes slower (or faster) than the kinetics of a process responsible for another type of fabric. The most important process for fabric development is deformation by the motion of crystalline dislocations. A fabric transition in such a case occurs when the dominant slip system changes, e.g.,

$$\dot{\varepsilon}_i(T, P, \sigma; f_{H_2O}, f_{O_2}, a_{MO}) = \dot{\varepsilon}_j(T, P, \sigma; f_{H_2O}, f_{O_2}, a_{MO}), \quad (1)$$

where $\dot{\varepsilon}_{i,j}$ is the strain rate due to the i-th or j-th slip system, T is temperature, P is pressure, σ is deviatoric stress, f_{H_2O} is water fugacity, f_{O_2} is oxygen fugacity, and a_{MO} is the activity of oxide. The fugacity of oxygen and the oxide activity in Earth's upper mantle do not change too much, so we ignore the influence of these factors on deformation fabrics. Also, to a good approximation, the influence of pressure can be included by the homologous temperature normalization for temperature (i.e., $\frac{T}{T_m(P)}$) and the normalization of stress by $\frac{\sigma}{\mu(P,T)}$, thus

$$\dot{\varepsilon}_i\left(\frac{T}{T_m(P)}, \frac{\sigma}{\mu(P,T)}; f_{H_2O}(P,T)\right) = \dot{\varepsilon}_j\left(\frac{T}{T_m(P)}, \frac{\sigma}{\mu(P,T)}; f_{H_2O}(P,T)\right), \quad (2)$$

where $T_m(P)$ is the melting temperature at pressure P, and $\mu(P, T)$ is the shear modulus at pressure P and temperature T. With this approximation, a fabric diagram showing the dominant fabric as a function of various parameters can be constructed in a three-dimensional space of $(\frac{T}{T_m(P)}, \frac{\sigma}{\mu(P,T)}; f_{H_2O}(P, T))$[4] as

$$G\left(\frac{T}{T_m(P)}, \frac{\sigma}{\mu(P,T)}; f_{H_2O}(P,T)\right) = 0. \quad (3)$$

Note that the function $G(\frac{T}{T_m(P)}, \frac{\sigma}{\mu(P,T)}; f_{H_2O}(P, T))$, which defines the fabric boundary, does not explicitly include strain rate. Therefore there is no need for corrections for difference in strain rate when the laboratory data are applied to geological problems as far as the flow laws are the same between deformation in laboratory studies and deformation in geological timescales. However, when flow laws are different between laboratory and in Earth, then the results of laboratory studies cannot be directly applied to Earth. There is no guarantee that the flow laws are the same between the laboratory studies and in Earth because the stress levels of laboratory deformation experiments tend to be higher than those operating in Earth. If the normalization of temperature and stress by $(\frac{T}{T_m(P)}, \frac{\sigma}{\mu(P,T)})$ is assumed, pressure does not have a direct effect. An intrinsic pressure effect would arise only when the normalization scheme $(\frac{T}{T_m(P)}, \frac{\sigma}{\mu(P,T)})$ is not valid.

Equation 1 means that if there is any difference in the dependence of strain rate on temperature, stress, or water content, then a fabric transition can occur when these variables change. In fact the first suggestion for the water-induced fabric transition, which was made by Karato (1995), was based on the observation by Mackwell et al.

[4]Although water fugacity is a function of pressure and temperature, it is also a function of total water content, and therefore the water fugacity is a variable that is in general independent of pressure and temperature.

(1985), who showed that the effect of water to enhance olivine deformation is highly anisotropic.

Equation 3 can be written more explicitly once the constitutive relationship for each slip system is known. A generic form for a flow law is (e.g., Karato 2008)

$$\dot{\varepsilon} = A \cdot \left(1 + B \cdot f_{H_2O}^{r}\right) \cdot \sigma^{n} \cdot \exp\left(-\frac{H^*}{RT}\left(1 - \left(\frac{\sigma}{\sigma_P}\right)^{q}\right)^{s}\right), \tag{4}$$

where A is a pre-exponential factor, B is a constant, σ_P is the Peierls stress, and q and r are nondimensional constants that depend on the process of dislocation glide. Two cases may be distinguished. First is the case in which the stress dependence of the activation enthalpy is small. This is the case for deformation at low stress (i.e., $\sigma/\sigma_P \ll 1$). In this case, Equation 4 is reduced to a power-law formula, $\dot{\varepsilon} = A \cdot (1 + B \cdot f_{H_2O}^{r}) \cdot \sigma^{n} \cdot \exp(-\frac{H^*}{RT})$. The fabric boundary corresponding to this case is given by

$$\frac{A_1 \cdot \left(1 + B_1 \cdot f_{H_2O}^{r_1}\right) \cdot \sigma^{n_1} \cdot \exp\left(-\frac{H_1^*}{RT}\right)}{A_2 \cdot \left(1 + B_2 \cdot f_{H_2O}^{r_2}\right) \cdot \sigma^{n_2} \cdot \exp\left(-\frac{H_2^*}{RT}\right)} = 1. \tag{5}$$

If the stress exponents for all slip systems are same (this is the case for olivine according to table 4 of Bai et al. 1991), then Equation 5 is reduced to

$$\log \frac{A_1}{A_2} \frac{1 + B_1 f_{H_2O}^{r_1}}{1 + B_2 f_{H_2O}^{r_2}} = \frac{H_1^* - H_2^*}{RT}. \tag{6}$$

A boundary corresponding to this case is sensitive to temperature and water content but not to stress. A fabric transition defined by this equation is called a class-I fabric transition.

Second is the case in which the stress dependence of activation enthalpy plays an important role. This is a case of deformation at high stress, low temperature. If the difference in the $(1 + B \cdot f_{H_2O}^{r}) \cdot \sigma^{n}$ term is ignored for simplicity, the fabric boundary is given by

$$\log \frac{A_1}{A_2} = \frac{H_1^*}{RT}\left(1 - \left(\frac{\sigma}{\sigma_{P1}}\right)^{q_1}\right)^{s_1} - \frac{H_2^*}{RT}\left(1 - \left(\frac{\sigma}{\sigma_{P2}}\right)^{q_2}\right)^{s_2}. \tag{7}$$

The fabric boundary defined by this equation is sensitive to stress and temperature but insensitive to water content. A fabric transition defined by this equation is called a class-II fabric transition.

The water fugacity term can in practice be replaced with the water content, C_W, which is readily measured. Both classes of fabric transition have been identified by the experimental studies (see below).

EXPERIMENTAL RESULTS

Plastic Anisotropy and Dominant Slip Systems in Olivine

The first extensive experimental studies on plastic deformation of olivine were reported in the early 1970s by Carter & Avé Lallemant (1970) and Phakey et al. (1972)

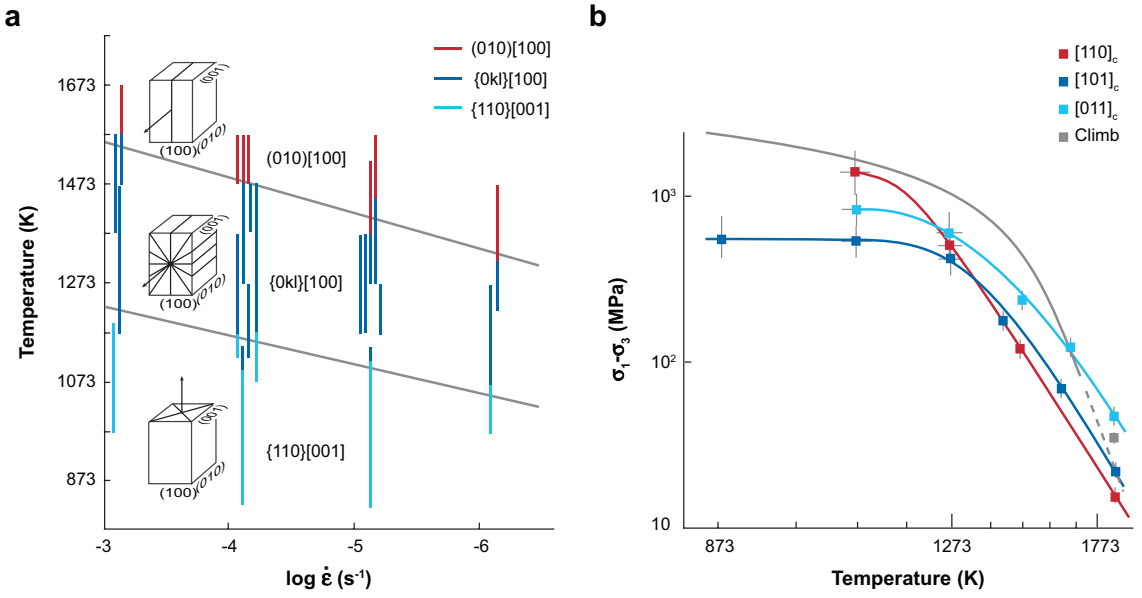

Figure 2

(*a*) Dominant slip systems in olivine as a function of strain rate and temperature (at P = 1.5 GPa) (from Carter & Avé Lallemant 1970). Results shown here suggest stress-induced transitions in the dominant slip systems, but the interpretation of these results is complicated because of the poor resolution of stress measurements and unknown water content (fugacity) (for details see text). (*b*) A comparison of creep strength for different orientations of single crystal and polycrystal at $\dot{\varepsilon} \approx 10^{-5}$ s^{-1} (from Goetze 1978). The $[110]_c$ activates the [100] (010) slip system, the $[101]_c$ orientation, the [100] (001) and [001] (100) slip systems, and the $[011]_c$ and [001] (010) slip systems.

on dunites (and lherzolites) and forsterite single crystals, respectively. In both studies, they used a Griggs-type solid medium apparatus under a broad range of conditions (P = 0.5–2.0 GPa, T = 900–1600 K, $\dot{\varepsilon} = 10^{-3}$–$10^{-6}$ s^{-1}). Carter & Avé Lallemant (1970) examined the slip systems mainly based on deformation microstructures at the optical microscope level, whereas Phakey et al. (1972) conducted extensive transmission electron microscope (TEM) studies to understand the microscopic mechanisms of deformation including the dominant slip systems. The results are summarized in **Figure 2** in which the results from the MIT group in the early to mid-1970s are also included. These studies show that (*a*) at high temperature and low strain rate, the dominant slip system in olivine is [100] (010); (*b*) at modest temperature and strain rate, the dominant slip direction remains [100], but slip occurs using many different slip planes; and (*c*) at low temperature and high strain rate, the dominant slip direction changes to **b** = [001] [slip plane is either (010) or (100) or both].

TEM: transmission electron microscopy

Phakey et al. (1972) noted that dislocations tend to be straight along the [001] direction in samples where **b** = [001] slip systems dominated, whereas dislocations are more curved at low stresses where **b** = [100] slip systems dominated. This

finding suggests that the control of dislocation motion by the Peierls potential is more important for the $\mathbf{b} = [001]$ slip systems than for the $\mathbf{b} = [100]$ slip systems.

The variation in the dominant slip systems with temperature and/or strain rate roughly corresponds to the variation in stress. As a result, these findings suggest that the dominant slip systems in olivine change with stress. However, there are two major complications in these earlier studies. First, because the solid-medium Griggs apparatus was used in these studies, friction between piston and the surrounding materials causes large uncertainties in the measured stress values (and hence the flow laws) (by as much as a factor of ~2 or more uncertainties in stress; e.g., Gleason & Tullis 1993). Although the above notion likely corresponds to stress-induced changes in the dominant slip system, the precise values of critical stress are poorly constrained by these studies. Second, the water content (or the fugacity of water) in these experiments is unknown. There was no report on the water content in the samples after these studies. The experience in our laboratory is that in most high-pressure experiments, some water is dissolved in olivine (and other minerals) unless extreme care is taken (see Huang et al. 2005, Nishihara et al. 2006, Wang et al. 2006). However, one important complication is that at high temperatures, where partial melting likely occurs, water tends to be removed from olivine because of the higher solubility of water into the melt, if the system is not saturated with water (e.g., Karato 1986). Some amount of water was likely present in these samples, but the exact amount is unknown. The water contents in samples deformed at temperatures exceeding the solidus (~1400–1500 K at these pressures) may have been systematically lower than those deformed at lower temperatures. This makes it difficult to interpret the significance of the results from these data, particularly those at high temperatures. However, the temperatures of 1100–1300 K, at which the transition to $\mathbf{b} = [001]$ slip systems occurs, is lower than the solidus, and hence the transition to $\mathbf{b} = [001]$ slip systems is likely due to high stresses.

The stress-induced changes in the dominant slip systems suggested by these earlier studies are not consistent with the later, low-pressure but more-precise experimental studies by Bai et al. (1991). Bai et al. (1991) conducted a series of deformation experiments on olivine single crystals at room pressure, $T = 1573–1773$ K (at various oxygen fugacity and oxide activity). They reported a complicated variation in the dependence of creep rate on temperature and chemical environment, but the stress exponents reported are essentially the same for all slip systems ($n = 3.5$) (Bai et al. 1991, table 4). If the same stress exponent applies to all the slip systems, then stress-induced changes in the dominant slip systems are not expected to occur, which is inconsistent with the stress-induced fabric transitions observed by Carter & Avé Lallemant (1970) and Jung & Karato (2001). One way to reconcile these conflicting observations is to invoke a transition from power-law creep behavior at low stress to the exponential flow law (Peierls mechanism) behavior at high stress as discussed by Goetze (1978), and Katayama & Karato (2006). In fact, **Figure 2*b*** shows that the temperature dependence of creep strength changes with temperature, which is consistent with the transition from power-law creep (at high temperature, low stress) to the Peierls mechanism (at low temperature, high stress). The transition in the relative

importance of dominant slip systems is caused by the difference in the temperature dependence of flow stress and temperature among different slip systems.

Mackwell et al. (1985) conducted an experimental study to examine the influence of water on deformation of olivine single crystals using a gas-medium apparatus at P = 0.3 GPa and T = 1573 K. Because the pressure is low, the influence of water on deformation is only modest and as a result the authors did not observe any changes in dominant slip systems in their studies. However, they found that the influence of water on the high-temperature plasticity is anisotropic: Deformation due to **b** = [001] dislocations is more enhanced than deformation involving **b** = [100] dislocations. Yan (1992) obtained similar results and showed that dislocation recovery is enhanced more for **b** = [001] dislocations than for **b** = [100] dislocations.

Earlier Experimental Studies on Olivine LPO

Avé Lallemant & Carter (1970) reported the results of LPO measurements of some samples from Carter & Avé Lallemant (1970). However, because they used an optical microscope technique to determine LPO, they only studied samples with large grain size, i.e., samples deformed at low stresses and high temperature. Nicolas et al. (1973) conducted a detailed study of deformation microstructures of water-poor synthetic olivine aggregates. In both cases, the deformation geometry was tri-axial compression, in which one can only identify the dominant slip plane but not the dominant slip direction. These studies reported that the olivine (010) plane becomes normal to the compression axis, which is consistent with the dominant role of the (010) plane as a slip plane. Combined with the results of transmission electron microscopy (TEM) and the observations of tilt walls by optical microscopy that indicate the dominant Burgers vector of **b** = [100], we consider that these observations correspond to the dominant slip system of [100] (010).

More details of LPO development can be investigated by simple shear deformation experiments in which the role of both the slip direction and the slip plane can be investigated. Also in a simple shear deformation geometry, one can deform samples to large strains, which is critical to the experimental study of LPO development. The first simple shear deformation experiments on olivine were made by Zhang & Karato (1995). They deformed synthetic water-poor olivine aggregates by simple shear deformation geometry. Their results are consistent with the previous notion that olivine [100] (010) is the dominant slip system at low stress and high temperatures.

Influence of Water

The experimental observations of the anisotropic enhancement of dislocation mobility in olivine by water suggest that the dominant slip systems in olivine may change with water content. However, the water fugacity in the experiments conducted by Mackwell et al. (1985) was low because of the low pressure, and the authors did not find any obvious changes in the dominant slip systems. By extrapolating these results to higher water contents, Karato (1995) proposed that the dominant slip systems (and hence the LPO) of olivine might change at high water contents and speculated that

the trench-parallel shear wave splitting observed in some subduction zones might be due to an unusual olivine fabric (the B-type fabric). To test this hypothesis, one needs to conduct quantitative large-strain deformation experiments in a low-symmetry geometry such as simple shear for a broad range of water fugacity. Recall that water solubility in minerals increases strongly with pressure (e.g., Kohlstedt et al. 1996). For example, water fugacity (at T = 1573 K) is ~0.3 GPa at P = 0.3 GPa, but it reaches ~55 GPa at P = 3 GPa and increases almost exponentially above this pressure. Consequently, important phenomena such as water-induced fabric transitions would occur only at high pressures. Also, because one of the predictions is the change in the dominant slip direction, one will need to conduct deformation experiments from which a change in slip direction can be detected from LPO measurements. Traditional tri-axial deformation experiments are not suited for this purpose because the slip direction is not uniquely identified from such experiments.

Thus, simple shear large-strain deformation experiments were conducted using a Griggs-type deformation apparatus at pressures exceeding those that can be achieved by a gas-medium deformation apparatus with a broad range of water contents (Jung & Karato 2001, Jung et al. 2006, Katayama et al. 2004, Katayama & Karato 2006). In all cases, water contents were determined after deformation experiments from a single crystal inserted into a part of the sample assembly oriented to inhibit deformation. An improved method for stress estimates is used, which is based on the calibration of the dislocation density and stress relationship (Karato & Jung 2003). A new high-resolution technique for dislocation density measurements was developed and used in these studies (Karato & Lee 1999), which yields stress estimates with an error of ±10%–15%. These technical improvements allowed us to conduct quantitative large-strain deformation experiments on olivine to pressures of ~2.2 GPa for a large range of water contents. To test the hypothesis of water-induced fabric transitions, deformation experiments were performed for different water contents but otherwise similar conditions [e.g., similar stress, similar (homologous) temperature]. These results largely confirm the earlier prediction by Karato (1995) and have provided a first dataset to quantitatively understand the influence of water content, temperature, and stress on olivine LPO.

Various deformation fabrics of olivine were identified in these studies (**Figure 3**). For each LPO, the corresponding dominant slip systems have been identified using the inverse pole figures (Jung et al. 2006). These inferences were further supported by the microstructural observations such as the Burgers vectors, the morphology of individual dislocations, and the geometry of sub-boundaries determined by optical microscopy as well as electron microscopy. The results are summarized in **Table 1**. They include the well-known fabric corresponding to the [100] (010) slip system (the A-type fabric), as well as other fabrics called the B-, C-, D-, and

Table 1 Relationship between the olivine fabric and the dominant slip systems

A-type	B-type	C-type	D-type	E-type
[100] (010)	[001] (010)	[001] (100)	[100] {0*kl*}	[100] (001)

Figure 3

Typical olivine LPOs found in the simple shear deformation experiments (figure modified after Jung et al. 2006).

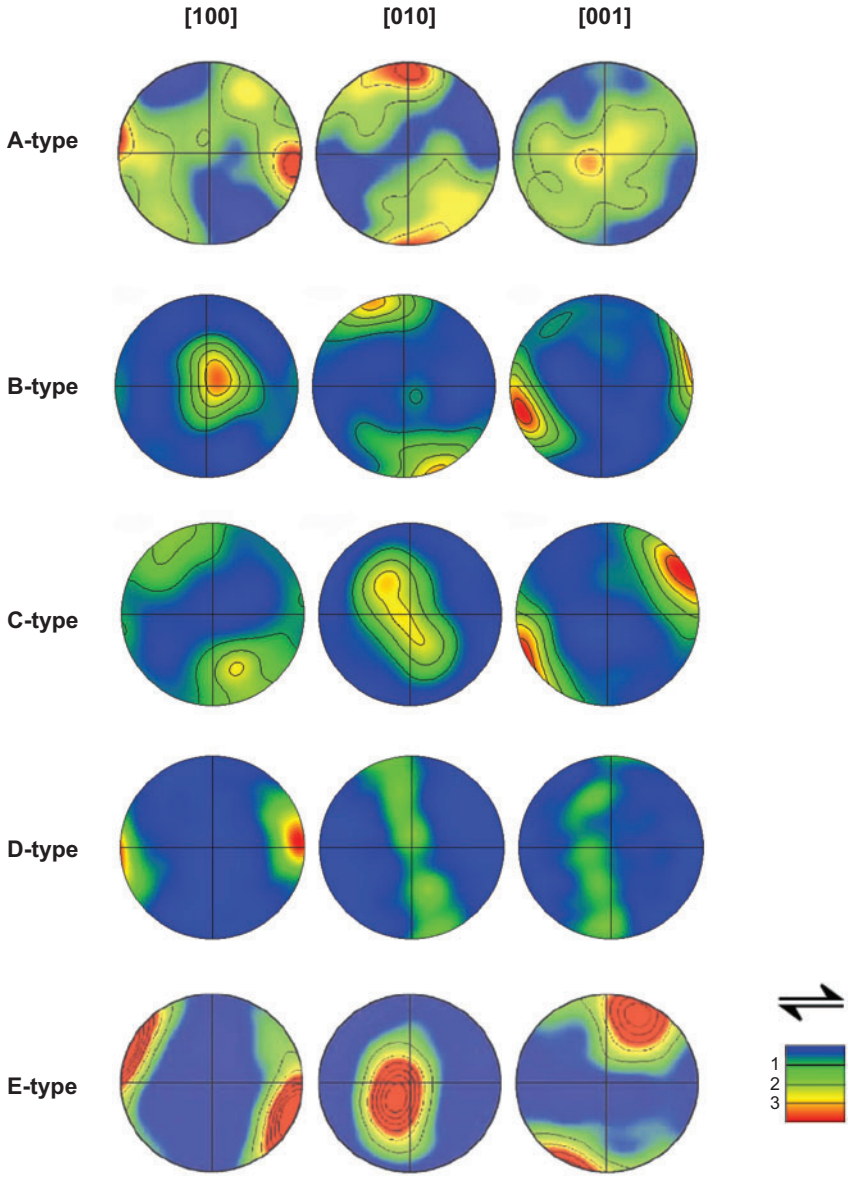

E-type fabric. Initial results were obtained at relatively high temperatures (T ~ 1470–1570 K) and the dominant olivine fabrics were studied as a function of water content and stress. Bystricky et al. (2001) conducted high-strain, shear deformation experiments on water-poor olivine aggregates similar to those conducted by Zhang & Karato (1995), but at higher stresses (at 0.3 GPa and 1473 K), and found a D-type olivine fabric under these conditions. Their results are in agreement with

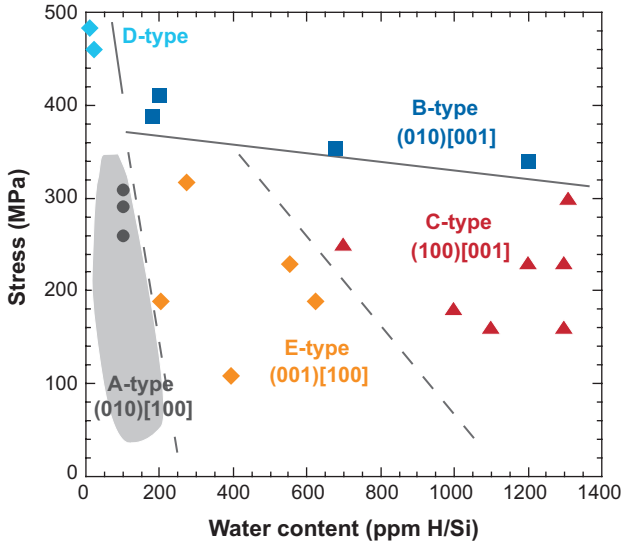

Figure 4

Deformation fabrics of olivine at high temperatures (T ~ 1470–1570 K) as a function of water content and stress (from Katayama et al. 2004). One of the data for D-type fabric is from Bystricky et al. (2001). Water content was estimated using the Paterson (1982) calibration. The values of water content will need to be modified if different calibrations are used [if the calibration from Bell et al. (2003) is used, the values of water content will be a factor of ~3 higher than shown in this diagram]. This correction for water content applies to **Figures 5** and **6** as well.

our results and those by Carter & Avé Lallemant (1970) (**Figure 2**), as shown in **Figure 4**.

The influence of temperature on the B- to C-type fabric boundary for a fixed water content (C_w~1500 ppm H/Si) was investigated by Katayama & Karato (2006). The high-temperature results for this boundary shown in **Figure 4** indicate that this transition is insensitive to water content but sensitive to stress, and therefore the results are interpreted using a model for the class-II fabric transition (**Figure 5**).

Together, these studies show that the fabric diagram for olivine must be constructed using at least three variables, namely, temperature, stress, and water content. **Figure 6** shows the dominant olivine LPOs as a function of normalized temperature, stress, and water content, ($\frac{T}{T_m(P)}$, $\frac{\sigma}{\mu(P,T)}$, C_W). Under lithospheric conditions[5] (low water content and modest stress and temperature), the A-type fabric dominates. However, when water content increases at high temperatures and at low stresses (i.e., asthenospheric conditions), the dominant olivine fabric changes first to E-type and then to C-type. B-type fabric is important above some critical stress that increases with temperature.

[5]Most of the LPO of minerals in the lithosphere is likely formed when materials are hot (i.e., shallow asthenospheric conditions) but at water-poor conditions after the removal of water by partial melting. This should be distinguished from deformation at deep asthenospheric conditions where water content is higher.

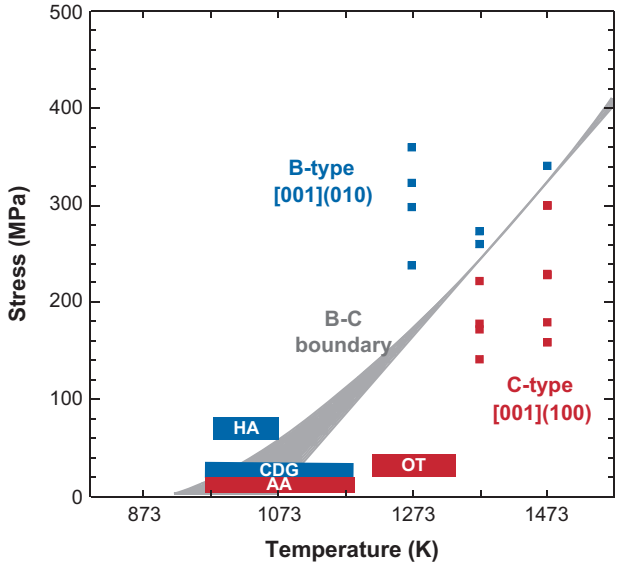

Figure 5

The influence of temperature and stress on the B-C boundary for olivine for a fixed water content ($C_w \sim$ 1500 ppm H/Si). Boxes indicate inferred deformation conditions for some naturally deformed peridotites with B- or C-type olivine fabrics. The gray band shows a range of stress-temperature conditions for the B-C boundary extrapolated from the experimental data using the exponential flow law (figure modified after Katayama & Karato 2006).

The A- to E-type fabric boundary, as well as the E- to C-type fabric boundary, is not sensitive to stress but sensitive to water content. Consequently, these transitions are interpreted as class-I transitions. In contrast, the fabric boundary between the B- and C-type fabrics is sensitive to stress and temperature but not to water content.

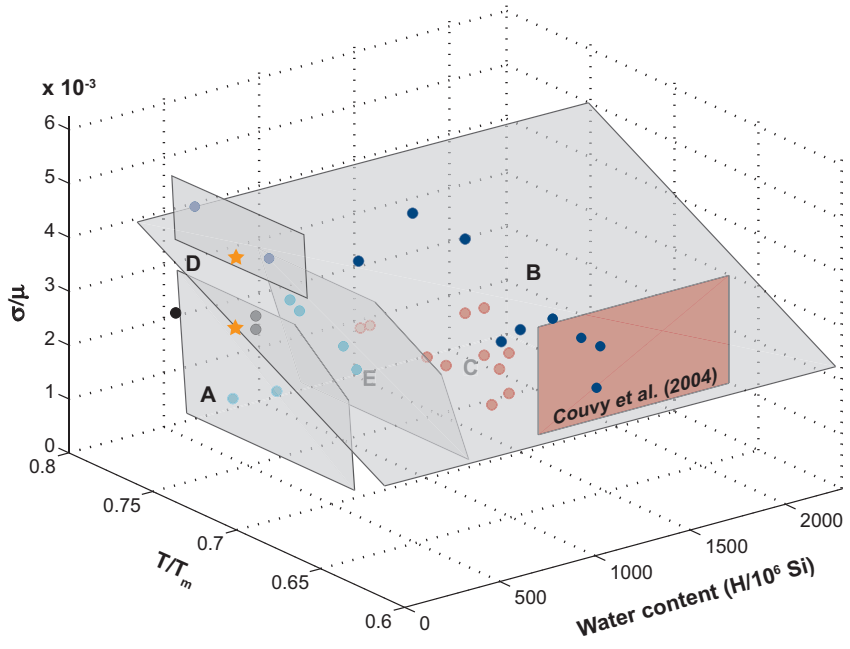

Figure 6

Olivine LPO in a three-dimensional space of $\left(\frac{T}{T_m(P)}, \frac{\sigma}{\mu(P,T)}, C_W\right)$.

This can be classified as a class-II transition. One of the immediate implications of these inferences is that the extrapolations of laboratory data on A- to E-type or E- to C-type fabric transitions to upper mantle conditions are justifiable if the laboratory experiments are conducted in the power-creep regime that likely dominates in Earth's upper mantle. Similarly, the B-type fabric likely dominates at low-stress and low-temperature conditions, although it is found only at very-high-stress conditions in high-temperature deformation experiments (Jung & Karato 2001, Katayama & Karato 2006).

Some details of the fabric diagram remain poorly constrained. For example, the temperature sensitivity of a fabric transition was investigated only for $C_w \sim 1500$ ppm H/Si. Also the extrapolation of the results on the B- to C-type transition to lower stress may not be secure because the exponential flow law would not be valid at low stress levels (see **Figure 5**). The fabric boundaries such as A- to E-type or E- to C-type transition are constrained only at relatively high stress conditions, and the temperature effects on these boundaries have not been investigated.

Influence of Pressure

The influence of pressure on deformation fabrics has not been fully explored. The series of studies conducted in our laboratory have allowed us to make the assumption that pressure influences olivine fabrics only through its effects on water fugacity and homologous temperature, and that there is no intrinsic effect of pressure on LPO. This assumption is based on the notion that a plausible intrinsic effect of pressure on plastic deformation in the pressure range of these studies is small compared with the influence of the variation in water fugacity.

Couvy et al. (2004) conducted simple shear deformation experiments of olivine at P = 11 GPa and T = 1673 K. They found that olivine fabric under these conditions is similar to the C-type fabric, and suggested that pressure changes the dominant slip system of olivine [essentially the same conclusion is proposed by Mainprice et al. (2005)]. However, two issues need to be addressed before such an interpretation can be accepted. First, because these are stress-relaxation tests, the exact values of stress at which much of LPO develops are unknown. The final stress was estimated from dislocation density and is as low as ~100 MPa, but the initial stress is on the order of ~1–2 GPa (Karato & Rubie 1997). Second, a significant amount of water (~2000 ppm H/Si) is detected in their samples after the experiments. In fact, when their results are plotted in a fabric diagram in three-dimensional space of $\left(\frac{T}{T_m(P)}, \frac{\sigma}{\mu(P,T)}; C_W\right)$ after normalization, their results fit into the C-type regime of the fabric diagram established by Jung & Karato (2001), Jung et al. (2006), Katayama et al. (2004), and Katayama & Karato (2006) (**Figure 6**). Therefore, we conclude that the experimental studies by Couvy et al. (2004) are consistent with our work and that they do not demonstrate the intrinsic effects of pressure on LPO.

Raterron et al. (2007) conducted a series of deformation experiments on water-free forestrite single crystals at P = 2.1–7.5 GPa and T = 1373–1677 K using a D-DIA (deformation-DIA) apparatus and reported that the dominant slip direction

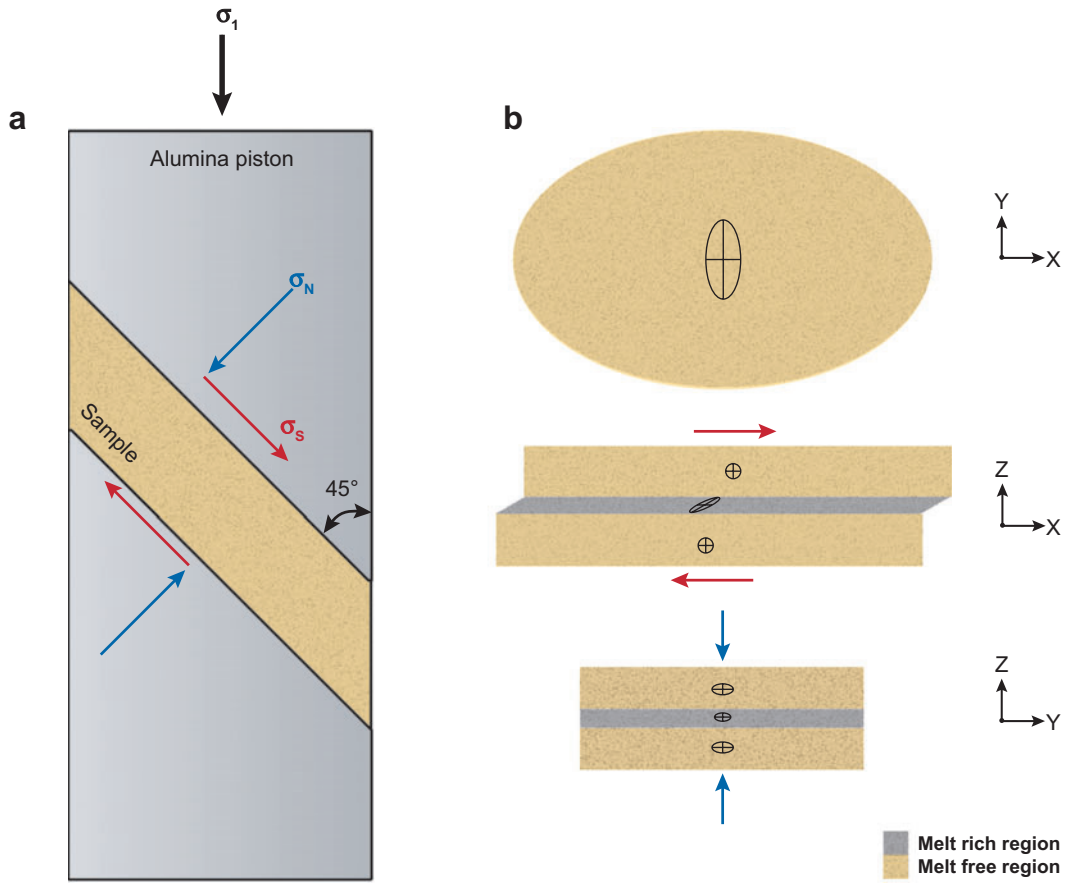

Figure 7

A schematic diagram showing the sample assembly and the deformation geometry in experiments by Holtzman et al. (2003). (*a*) Axial compression is converted to nearly simple shear deformation of the bulk of a sample in this assembly, with a small additional component of compressional deformation (see Zhang & Karato 1995, Zhang et al. 2000). (*b*) Geometry of deformation of the melt-free region and the melt-rich regions is different if shear deformation is localized in the melt-rich region (X, shear direction; Y, normal to the shear direction in the shear plane; and Z, shear plane normal). Deformation of the melt-free region, which is volumetrically dominant and is responsible for olivine LPO, is dominated by deformation caused by compression. In this model, the anisotropic flow due to compression is caused by the oblate shape of the sample and is an artifact of this experimental setup.

changes from **b** = [100] to [001] above ~5 GPa. However, all their experiments were conducted at stresses higher than 200 MPa. Goetze (1978) showed that at stress higher than ~200 MPa the dominant mechanism of deformation in olivine switches to the Peierls mechanism, and that at these stress levels the **b** = [001] slip systems dominate over the **b** = [100] slip systems (see **Figure 2**). Consequently, the results by Raterron et al. (2007) can also be interpreted as stress-induced slip system change

in olivine (e.g., Carter & Avé Lallemant 1970, Goetze 1978) and do not demonstrate the intrinsic effect of pressure on the relative importance of the slip systems.

Durinck et al. (2005) reported the results of theoretical calculations on the resistance to slip in olivine for various slip systems as a function of pressure (at T = 0 K). They found the slip with **b** = [001] slip systems becomes easier than slip by **b** = [100] slip systems as pressure is increased, and argued that pressure may change the dominant slip system in olivine. However, the interpretation of these calculations is problematic for the following reasons. First, and most importantly, in this work they calculated the resistance to homogeneous shear and ignored the influence of localized deformation (i.e., concept of dislocations). Actual resistance for deformation at T = 0 K (the Peierls stress) is controlled largely by the localized deformation on a dislocation line (Peierls 1940), and therefore the validity of the approach taken by Durinck et al. (2005) is questionable. Second, even if one calculates the Peierls stress for various slip systems correctly, the application of these results to high-temperature deformation is not straightforward because high-temperature creep involves various processes including kink nucleation/migration, cross-slip, and dislocation climb (Karato 2008, Poirier 1985). If creep rate is controlled by diffusion-controlled dislocation climb under jog-saturated conditions as proposed by Kohlstedt (2006), then the results of calculations by Durinck et al. (2005) would be irrelevant to fabric transitions.

In summary, although substantial progress has been made toward our understanding of fabric development at high pressures, there are no conclusive studies at this time that demonstrate any intrinsic influence of pressure on olivine LPO. Instead, the currently available data on LPO in olivine can be summarized using the three-dimensional space ($\frac{T}{T_m(P)}$, $\frac{\sigma}{\mu(P,T)}$; C_W), and as far as this normalization applies, there is no explicit pressure dependence on the development of LPO. However, existing studies do not preclude intrinsic effects of pressure on LPO either. To demonstrate any intrinsic pressure effect beyond the normalization (i.e., exceptions to that normalization scheme), one would need to conduct large-strain deformation experiments at various pressures, keeping other factors (such as stress and water content) close to the similar values.

According to the hypothesis of a pressure-induced fabric transition in olivine, olivine fabrics will change to a C- (or B-)type fabric when pressure reaches a certain critical value. Raterron et al. (2007) estimate this value to be ∼5–7 GPa depending on the temperature. However, observations on olivine LPO from samples deep in the upper mantle are not consistent with this view. First, Jin (1995) investigated the deformation microstructure of one of the ultradeep (>300 km) peridotites discovered by Haggerty & Sautter (1990). One of the peridotite samples (JAG 84–318) with a coarse granular texture (grain size is ∼2–4 mm) shows a relatively strong A-type olivine fabric. Because the stress level inferred from the grain size is low (∼2–3 MPa), the deformation that resulted in olivine fabric is likely to have occurred in the deep upper mantle condition [∼300 km (∼10 GPa)]. Second, most sheared lherzolites that came from 150–200 km and hence were deformed at pressures at ∼5–6 GPa show A-type olivine fabrics (P. Skemer, 2007, personal communication). These observations are not consistent with the idea of pressure-induced fabric transition proposed by Raterron et al. (2007) and Mainprice et al. (2005).

Influence of Partial Melting

Using a high-pressure simple shear deformation technique developed by Zhang & Karato (1995), Zimmerman et al. (1999) and Holtzman et al. (2003) performed shear deformation experiments on olivine + melt systems at P = 0.3 GPa and T = 1523 K. When olivine + basalt is deformed with a small amount of water, deformation is nearly homogeneous, and the LPO is the same as that of a melt-free olivine (A-type fabric). However, when melt permeability is reduced by the addition of other materials such as chromite spinel or FeS, much of the imposed shear strain is accommodated by deformation in melt-rich bands, and the olivine LPO is different from that of melt-free olivine: Olivine [100] axes are concentrated toward normal to the macroscopically imposed flow direction on the flow plane, and olivine [001] axes are aligned along the shear direction, a fabric similar to the olivine B-type fabric. A TEM study of these samples showed that the dominant Burgers vector (slip direction) of olivine in these samples is $\mathbf{b} = [100]$, and consequently Holtzman et al. (2003) interpreted this observation as due to the change in the deformation geometry of the solid component: In these experiments, the strain geometry of the solid component is orthogonal to that of the imposed macroscopic strain (**Figure 7**). They further postulated that such strain partitioning occurs in a natural setting, and proposed that some of the trench-parallel shear wave splitting observations might be due to this process.

If such strain partitioning is fundamental to deformation of partially molten materials (with localized shear), then the argument by Holtzman et al. (2003) for the application of such results to Earth's mantle would be justified. However, as illustrated in **Figure 7**, the cause for such strain partitioning is likely the anisotropic geometry of the sample in their particular experimental setup. They adopted the shear deformation setup developed by Zhang & Karato (1995), in which axial compression causes simple shear and a small degree of compression of a sample. If shear deformation is localized in the melt-rich regions and the melt-free region does not deform much by shear, then deformation of the melt-free region is dominated by compression and the geometry of compressional deformation will control the geometry of LPO. The compressional component of deformation in this sample geometry occurs by the flow of sample between two pistons caused by the pressure gradient. Owing to the oblate shape of the sample, the pressure gradient is anisotropic: Flow normal to the imposed shear direction is stronger than the flow parallel to the shear direction (**Figure 7**) (otherwise the flow will be axially symmetric).

According to this interpretation, the olivine fabric that Holtzman et al. (2003) observed is an experimental artifact and it is difficult to justify the application of these experimental observations to natural environments such as mid-ocean ridges or subduction zones. In addition, trench-parallel shear wave splitting is frequently observed in forearc regions (e.g., Nakajima & Hasegawa 2004) where partial melting is unlikely to occur. The observations by Holtzman et al. (2003) of olivine LPO are most likely an experimental artifact and do not apply to natural settings, particularly to the forearc region of subduction zones where trench-parallel shear wave splitting is often observed.

Perhaps the most important factor by which partial melting could modify olivine LPO is the redistribution of water. As first pointed out by Karato (1986), partial melting likely removes water from minerals such as olivine when partial melting occurs under water-undersaturated conditions. In Earth's asthenosphere or in plume roots, the water content is expected to exceed the critical value for E- or C-type fabric but remain below the saturation limit. Upon partial melting, much of the water structurally bound in minerals will be partitioned into the melt and will cause a fabric transition from an E- or C-type fabric to an A-type fabric. Some of the implications of this type of fabric transition are discussed below.

LPO of Orthopyroxene and Other Minerals

A typical upper mantle peridotite contains ~40%–60% of olivine, ~20%–30% of orthopyroxene, 0%–15% clinopyroxene, ~0%–20% of garnet, and 0%–5% spinel depending on the depth and the bulk chemical composition (e.g., Ringwood 1975). Therefore, under some conditions, orthopyroxene and other minerals may contribute significantly to seismic anisotropy (Skemer et al. 2006). In contrast to the large number of experimental and theoretical studies on the development of olivine fabrics, relatively few studies have investigated orthopyroxene LPO. Virtually all naturally deformed peridotites have LPOs consistent with deformation on the [001] (100) slip system (Christensen & Lundquist 1982, Mercier 1985). In particular, the orthopyroxene LPO in the samples from Cima di Gagnone (Switzerland) is the same as the well-known fabric from other localities despite the fact that olivine LPO from this region shows B- and C-type fabrics. This suggests that water may not have an influence on orthopyroxene LPO, although this has yet to be tested experimentally.

The persistence of $\mathbf{b} = [001]$ slip in orthopyroxene can easily be understood from the crystal structure: The length of $\mathbf{b} = [001]$ in orthopyroxene is much shorter than those of other Burgers vectors. However, dominant slip planes can change under some conditions. For example, in a peridotite from Lherz, French Pyrenees, Avé Lallemant (1967) and Carter et al. (1972) reported orthopyroxene LPOs in which orthopyroxene [010] is perpendicular to the foliation plane, suggesting a dominant slip on the (010) plane. The (010) slip was also found in a series of tri-axial deformation experiments by Carter et al. (1972), who found orthopyroxene [010] parallel to the maximum compression direction and the [100] and [001] axes forming girdles in the plane normal to the maximum compression. Slip on both the (100) and (010) planes was identified in the experiments by Ross & Nielsen (1978), although the observed LPO was influenced primarily by the (100) plane. The thesis by George (1975), as reported in Mercier (1985), also found [100] axes parallel to the compression direction in tri-axial deformation experiments, consistent with slip on the (100) plane. In spite of the few exceptions, there appears to be minimal variation in orthopyroxene fabrics in nature. This may be a useful property of orthopyroxene, as its fabrics may be used to infer the geometry of deformation, even if no other kinematic indicators are present.

However, contributions to seismic anisotropy from orthopyroxene and other secondary minerals are usually not large except for cases in which anisotropy caused

by olivine is weak (Christensen & Lundquist 1982). Consequently, in this review we focus mainly on olivine LPOs for which there are a number of new observations. However, a refined analysis of seismic anisotropy will require the incorporation of contributions from these secondary minerals. For seismic anisotropy caused by these minerals see Mainprice et al. (2000).

DISCUSSION

Microscopic Mechanisms of (Water-Induced) Fabric Transitions

Because deformation fabrics (LPO) develop by large-strain deformation involving dislocation glide, an obvious cause for the fabric transitions is the change in the dominant slip systems. Indeed, the analysis of inverse pole figures as well as microstructural observations on dislocations strongly support the transition in the dominant slip systems (Jung et al. 2006). Numerical modeling by Kaminski (2002) confirmed this point by showing that olivine LPO changes when the relative importance of different slip systems is modified.

The next question is why and how the dominant slip systems change with physical and chemical conditions, as observed in laboratory studies by Jung & Karato (2001), Jung et al. (2006), and Katayama & Karato (2006). To answer this question, one must understand not only why and how water enhances plastic deformation of olivine but also why the influence of water is different for different slip systems. For example, if the cause for enhancement of deformation by water is simply due to the enhancement of diffusion as proposed by Kohlstedt (2006), then one cannot explain the observed anisotropy in the enhancement of deformation. Indeed, the fact that deformation of $\mathbf{b} = [001]$ slip is more enhanced by water is not consistent with this model for the following reasons. TEM studies discussed above show that for $\mathbf{b} = [001]$ slip, dislocations are mostly screws, indicating that the motion of screw dislocations is more difficult than that of edge dislocations. Motion of screw dislocations is in most cases conservative and does not involve diffusion (e.g., Nabarro 1967). Furthermore $\mathbf{b} = [001]$ screws in olivine are mostly straight, indicating the important role of the Peierls stress. Therefore, the diffusion-control model proposed by Kohlstedt (2006) is not supported by the observations.

High anisotropy in the water effects suggests that the effect is closely related to crystallographically controlled properties of a dislocation. Two possibilities can be imagined: (*a*) the role of jogs on edge dislocations that affect the rate of dislocation climb, and (*b*) the role of kinks that control the rate of dislocation glide (+ control by the motion of jogged screw dislocations). These models may be compared with the experimental observations of class-I and class-II fabric transitions. In class-II fabric transitions, stress dependence of activation enthalpy plays an important role, and this model is consistent with a Peierls-stress-controlled model of creep: Kink density and/or mobility is modified by the addition of water, possibly through the reduction of kink energy as discussed by Heggie & Jones (1986). In fact, I. Katayama & S.-I. Karato (manuscript submitted, 2007) reported experimental results on olivine

showing the reduction of the Peierls stress by water. The class-I behavior is likely due to the increase in jog density by water, assuming that creep is controlled by dislocation climb under jog-undersaturated conditions (e.g., Karato & Jung 2003, Mei & Kohlstedt 2000). Again, if dislocation self-energy is reduced by hydration, then jog density will increase. Both processes are likely anisotropic and the reduction of Peierls energy is likely higher for the dislocations with a longer Burgers vector ($\mathbf{b} = [001]$). This finding provides a reasonable explanation for anisotropic enhancement of plastic deformation in olivine that leads to fabric transitions. More detailed TEM observations on dislocations are needed to examine these models. Influence of hydration on dislocation splitting, as first proposed by Drury (1991), is another process that may play a role(s) in enhancing dislocation glide.

Comparison to Geological Observations

In one of the first reports on olivine LPO, Yoshino (1961) reported olivine B- and C-type fabrics in deformed peridotites from the Sambagawa metamorphic belt, Japan. Similarly, Möckel (1969) reported olivine C-type fabrics from a naturally deformed peridotite in the Swiss Alps (see also Buiskool Toxopeus 1976). These reports were ignored as anomalous (unimportant) fabrics in most of the recent olivine LPO literature (e.g., Ben Ismail & Mainprice 1998) because the origin of these fabrics was unknown. Dobrzhinetskaya et al. (1996) argued that the olivine fabric in the peridotite from Alpe Arami is so unusual (C-type fabric) that it might be inherited from a fabric developed in the transition zone. In contrast, a large number of peridotite samples show A-type olivine fabrics (e.g., Ben Ismail & Mainprice 1998, Nicolas et al. 1971), which led to a notion that olivine A-type fabric is the most important fabric in the upper mantle, and most seismic observations have been interpreted using the olivine A-type fabric.

However, the frequency of peridotite samples observed on Earth's surface should not be considered the frequency of these samples in Earth's upper mantle. Peridotite samples that we observe on Earth's surface are transported to the surface by particular geological processes, which imposes a sampling bias on the geological observations. An important geological process that will modify rheological properties and hence the deformation fabrics of peridotites is the depletion of water by partial melting (e.g., Karato 1986). Peridotites near the surface (i.e., the lithosphere) have been subjected to partial melting and have lost much of their water, and much of their strain was likely to have accumulated after dehydration when they are still hot (in the shallow asthenosphere). This leads to a layering in which depleted (water-poor) peridotites dominate in near-surface regions (the lithosphere), whereas undepleted (water-rich) peridotites occur in the deeper upper mantle (deep asthenosphere). These peridotites that were deformed at water-poor and hot conditions (and that preserve frozen microstructures) are frequently observed on Earth's surface. Undepleted water-rich peridotites are likely volumetrically abundant in the deep upper mantle and play important geodynamic roles, but they are rarely sampled on Earth's surface. Given these considerations, we should interpret the observations of deformation fabrics of various

peridotite samples on Earth's sample only as an illustration of possible fabric types that may occur in Earth's interior. We should not use these observations to directly infer the frequency of various fabric types in Earth.

Another complication in using the observations of naturally deformed peridotites is that although deformation fabrics (LPO) are difficult to modify through the transportation process to the surface, water content is likely modified during transportation. This is due to the fast kinetics of diffusion of hydrogen (and related species). Consequently, the observed water content of a given natural sample cannot be used to infer the water content of the sample during the plastic deformation that generated the LPO (e.g., Karato 2006).

In addition, it is not straightforward to infer the temperature and pressure conditions at which large strain plastic deformation that caused LPO occurred. Conventional geothermometry and geobarometry provide the temperature and pressure at which the distribution of some elements (Al, Ca, Mg, Fe) among coexisting minerals attained the final chemical equilibrium. However, these temperature and pressure conditions do not necessarily correspond to the temperature and pressure conditions at which large-strain plastic deformation occurred to form deformation fabrics. [Mizukami et al. (2004) conducted a careful microscale chemical analysis to infer the temperature at which dynamic recrystallization (deformation) occurred]. The characteristic time for chemical equilibrium is shorter than that of large-strain deformation, and large-strain deformation could have occurred at temperature and pressure conditions different from those recorded in element distribution.

Given these limitations, the significance of observations on deformation fabrics in peridotites cannot be evaluated easily. However, the existing observations may be summarized as follows.

- Most peridotite samples from ophiolites (oceanic lithosphere) and the continental lithosphere show A-type olivine fabrics. (Some peridotites in ophiolites that were deformed at low temperature and high stress show D-type fabrics.)
- Some peridotite samples collected from convergent boundaries (e.g., Buiskool Toxopeus 1976, Dobrzhinetskaya et al. 1996, Frese et al. 2003, Mizukami et al. 2004, Möckel 1969, Skemer et al. 2006) show B- or C-type fabrics.
- Samples from the deep upper mantle show a range of olivine fabrics including A- and C-types (e.g., Jin 1995, Katayama et al. 2005, Xu et al. 2006).
- A few samples from collision zones and from island arc environments show E-type fabrics (e.g., Mehl et al. 2003, Sawaguchi 2004).

These observations are consistent with the experimental results, which show a diversity of olivine fabrics corresponding to a variety of stress, water content, and temperature conditions. The dominance of the A-type olivine fabric in the lithosphere is consistent with the experimental observations (we assume that the deformation fabrics of most of the peridotites in the lithosphere are formed in the shallow asthenosphere after the removal of water by partial melting). The observations of C-type samples in collision zones and from the deep upper mantle are consistent with the experimental observations showing that C-type olivine fabric is formed under water-rich conditions. In more detail, the variability of fabric types may be interpreted in terms

of regional variation in some parameters such as temperature and water content. For example, Katayama & Karato (2006) interpreted the B- and C-type fabrics observed in naturally deformed peridotites in terms of the regional variation in temperature at which the deformation fabrics were formed (**Figure 5**).

Although the laboratory data and the estimated water content from geochemical and geophysical observations would suggest that E-type (or C-type) fabric should be widespread in the asthenosphere, E-type fabric is only rarely observed. This may simply be a result of highly incomplete sampling of peridotites from the deep upper mantle. More extensive studies are needed to obtain a better idea about the role of water and perhaps of pressure on deformation fabrics of olivine (and other minerals). The application of laboratory data to geological conditions (lower stresses) is not always straightforward. For example, although the results of such an extrapolation seem to agree with observations on natural samples (see **Figure 5**), extrapolation of exponential flow law to low stress is not justified, and the exact fabric boundary for the B- to C-type transitions at low stress levels is poorly constrained at this time.

In summary, the new laboratory results summarized in **Figure 6** provide the first explanation for some of the anomalous olivine fabrics. On the basis of these new experimental observations, we believe peridotites with these anomalous olivine fabrics are from water-rich (deep) regions that are not normally exposed at Earth's surface. Combined with other lines of inference, we argue that these samples, although they are rare on Earth's surface, may represent a large portion of Earth's deep upper mantle. However, the applicability of such a diagram to low-stress conditions is not clear and the nature of fabric boundaries at geological conditions still has some uncertainties.

Interpretation of Seismological Observations

In addition to the observations on naturally deformed rocks, seismological observations of anisotropic wave propagation (seismic anisotropy) provide additional constraints on the influence of deformation environments (stress, water content, temperature, etc.) on deformation fabrics. We discuss some of the seismological observations that may be interpreted in view of our new results on olivine LPO.

Seismic anisotropy in subduction zones. Water is transported into the mantle by subducting slabs. Consequently, the interpretation of seismic anisotropy in the subduction zones must incorporate the new results on the influence of water on olivine LPO. Also, a wide range of temperature is expected in the subduction zone because a cold slab and hot mantle meet there. One of the remarkable observations on the upper mantle near subduction zones is that close to the trench the polarization of fast shear waves is nearly trench-parallel, but nearly trench-normal further toward the back arc (e.g., Long & van der Hilst 2005, Nakajima & Hasegawa 2004, Smith et al. 2001) (**Figure 8*a***). If the old paradigm of the olivine A-type fabric were used to interpret such an observation, then the observed geometry of anisotropy would imply trench-parallel flow close to a trench and trench-normal flow away from a trench. Some authors invoked trench migration as a cause of trench-parallel flow near a trench (e.g., Buttles & Olson 1998, Russo & Silver 1994, Smith et al. 2001). However, it is not

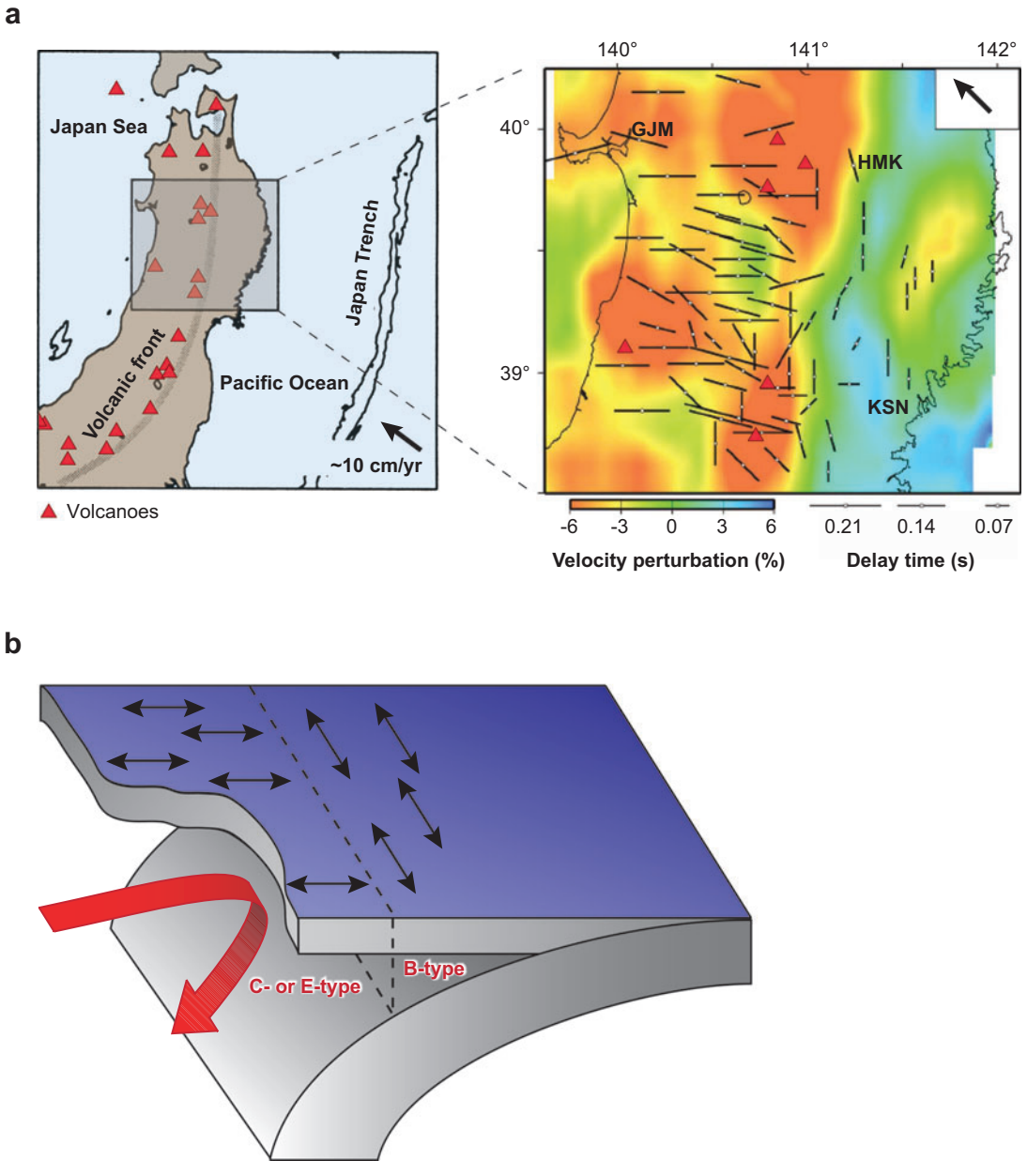

Figure 8

(*a*) Fast shear wave polarization in Tohoku, Japan, showing trench-parallel polarization near the trench that rotates nearly trench-normal behind the volcanic arc (Nakajima & Hasegawa 2004). (*b*) A model to explain the seismological observations in terms of temperature and stress distribution corresponding to simple slab-induced flow in the mantle wedge (modified after Kneller et al. 2005).

easy to have trench-parallel flow for a broad range of conditions because the velocity of trench migration is in most cases much smaller than the velocity of slab subduction.

An alternative model to explain trench parallel fast shear wave splitting is transpression (e.g., Nicolas 1993). When a layer of soft materials sandwiched between strong materials is compressed obliquely to the layer, then deformation of the soft layer occurs more or less parallel to the layer itself. There is strong geological evidence that shallow portions of collision zones undergo this mode of deformation (Nicolas 1993). However, because transpression occurs only under particular conditions, it is not obvious that this mode of deformation can penetrate deep into the mantle. Furthermore, in Tohoku, Japan, where a clear transition from trench-parallel to trench-normal occurs (Nakajima & Hasegawa 2004), the direction of subduction is almost exactly normal to the trench. In addition, geodetic observations based on GPS in this area do not show any change in trend across the region where shear wave splitting changes its pattern (A. Hasegawa, private communication). Therefore, we consider transpression to occur only in limited regions or over a limited depth range (shallow upper mantle), and the large portion of seismic anisotropy to be due to anisotropic structure in the deeper upper mantle.

Currently, our preferred explanation for the spatial distribution of anisotropy in the subduction zone is the variation in olivine fabrics due to the variation in stress and temperature (with the presence of some water) as proposed by Jung & Karato (2001) and Karato (1995, 2003b) (**Figure 8*b***). Results of detailed numerical modeling by Kneller et al. (2005, 2007) provide support for this model and suggest that the coupling between subducting lithosphere and the materials above plays a key role in controlling the distribution of anisotropy through the control of the temperature (and stress) distribution of the wedge mantle. In this model trench-parallel fast shear wave polarization is attributed to the B-type olivine fabric associated with nearly vertical flow in the relatively cold regions of mantle wedge (see also **Table 2**). Because B-type fabric develops only at low temperatures, subduction of a young and hence hot lithosphere would not cause B-type fabric in a large region. Seismological observations on different subduction zones will be useful to address this point.

Using the observations on teleseismic (SKS) waves, Russo & Silver (1994) argued that the trench-parallel fast shear wave polarization in South America is due to the flow beneath the subducting lithosphere, and in such a case our model would not explain the observations. However, because the shear wave splitting observations from SKS waves do not have depth resolution for the location of anisotropic structure, interpretation of such observations remains elusive.

Although not much seismological data are available, recent laboratory results also suggest that anisotropy in the deep upper mantle of subduction zones likely reflects regional variations in water content. Indeed, Shito et al. (2006) presented some evidence for the spatial variation in water content in the deep mantle wedge (~300 km deep) in the Philippine Sea region. If detected, spatial variations in anisotropy in the deep mantle wedge would also provide constraints on the distribution of water.

Seismic anisotropy of the asthenosphere and plumes. The water content of the (deep) asthenosphere (source region of mid-oceanic basalt) can be estimated from

Table 2 Relation between olivine fabrics and seismic anisotropy corresponding to various flow geometries

Shear wave splitting (direction of the polarization of the faster, vertically traveling shear wave)		
Fabric	**Horizontal flow**	**Vertical planar flow**
A-type	Parallel to flow	Small splitting
B-type	Normal to flow	Parallel to the plane
C-type	Parallel to flow	Normal to the plane
D-type	Parallel to flow	Small splitting
E-type	Parallel to flow	Small splitting
V_{SH}/V_{SV} **anisotropy**		
Fabric	**Horizontal flow**	**Vertical cylindrical flow**
A-type	$V_{SH}/V_{SV} > 1$	$V_{SH}/V_{SV} < 1$
B-type	$V_{SH}/V_{SV} > 1$	$V_{SH}/V_{SV} > 1$ (weak)
C-type	$V_{SH}/V_{SV} < 1$	$V_{SH}/V_{SV} > 1$ (weak)
D-type	$V_{SH}/V_{SV} > 1$	$V_{SH}/V_{SV} < 1$
E-type	$V_{SH}/V_{SV} > 1$ (weak)	$V_{SH}/V_{SV} < 1$

the water content of mid-ocean ridge basalt and is ~100 ± 50 ppm wt (~1500 ± 800 ppm H/Si) (e.g., Hirschmann 2006). The inference of water content from electrical conductivity measurements gives a somewhat smaller but similar value (Wang et al. 2006). If these results and the inferred temperature (and pressure) of the asthenosphere are used, the olivine LPO in the asthenosphere (and deep upper mantle) is likely E- or C-type, and likely not A-type. This conclusion is different from the conventional view in which all observations of seismic anisotropy in the upper mantle are due to the A-type olivine fabric (e.g., Becker et al. 2003, Savage 1999). Note, however, that the uncertainties in the water content estimated from a petrological approach or from electrical conductivity are large (there is also an issue of water content calibration, which will affect the water content shown in **Figures 4**, **5**, and **6**). It is not possible to predict from such methods whether E- or C-type fabric is present in the oceanic asthenosphere. If one can infer the type of anisotropy in the oceanic asthenosphere, then one would obtain a tighter constraint on the water content in the asthenosphere.

The best method to address this question would be to examine the olivine fabric from materials of (deep) asthenospheric origin. However, almost all peridotite samples are from the lithosphere, and there is no report of olivine fabrics in an asthenospheric peridotite (at least from the deep asthenosphere before the depletion of water by partial melting). An alternative approach is to investigate the details of the seismological signature. The olivine C-type fabric shows $V_{SV} > V_{SH}$ anisotropy for horizontal shear (see **Table 2**) that is not consistent with the seismological observation for the oceanic asthenosphere (e.g., Montagner & Tanimoto 1990, 1991). Therefore, the real question is whether the oceanic asthenosphere has the olivine A- or E-type fabric. At a qualitative level, olivine A- and E-type fabrics result in a similar seismological signature (see **Table 2**): Both fabrics show the fast S-wave polarization direction

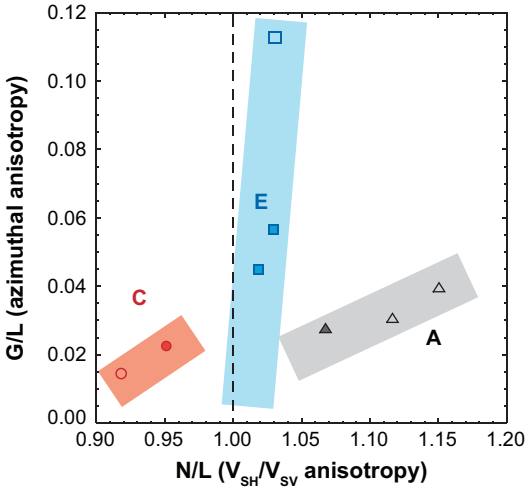

Figure 9

The relation between azimuthal and polarization anisotropy caused by various types of olivine LPO. Horizontal shear flow is assumed. $G/L \approx (\Delta V/V)^2$, where $\Delta V/V$ is the magnitude of azimuthal anisotropy of shear waves [e.g., shear wave splitting; dominance of 2θ (θ: azimuth) term is assumed] and $N/L = (V_{SH}/V_{SV})^2$. Solid symbols: experimental samples (from Jung et al. 2006), open symbols: natural samples.

parallel to the flow direction, and horizontal shear produces $V_{SH} > V_{SV}$ anisotropy. However, upon closer examination there are some differences. The main difference between the A- and E-type fabrics is the olivine orientation along the vertical axis. If horizontal shear is assumed in the asthenosphere, olivine [010] axes will be vertical in an A-type fabric but olivine [001] axes will be vertical in an E-type fabric. This results in differences in the strength of azimuthal and polarization anisotropy, as shown in **Figure 9**. Olivine E-type fabrics would result in stronger azimuthal anisotropy (e.g., amplitude of shear wave splitting) and weaker V_{SH}/V_{SV} anisotropy than the A-type fabric. There are some findings to support this hypothesis. First, the amplitude of V_{SH}/V_{SV} anisotropy in the asthenosphere is generally smaller than that of the lithosphere (e.g., Montagner & Tanimoto 1990, 1991). If olivine A-type fabric is important in both the lithosphere and asthenosphere because the strain magnitude is larger in the asthenosphere than in the lithosphere, one would expect stronger anisotropy in the asthenosphere (e.g., Tommasi 1998). One way to explain a weak V_{SH}/V_{SV} anisotropy in the asthenosphere is to invoke the E-type olivine fabric. Another observational test would be to see if the azimuthal anisotropy is stronger in the asthenosphere than in the lithosphere. If the A-type fabric is dominant in the asthenosphere, one expects stronger azimuthal anisotropy in the asthenosphere than in the lithosphere (because of a larger strain in the asthenosphere than in the lithosphere). In contrast, if the E-type fabric is dominant in the asthenosphere (but the A-type is dominant in the lithosphere), then the azimuthal anisotropy in the asthenopshere should be weaker than that in the lithosphere. Measuring azimuthal anisotropy is difficult, but several findings support this hypothesis. First, Debayle et al. (2005) reported that the amplitude of azimuthal anisotropy in the asthenosphere is stronger than that in the lithosphere in oceanic regions. Second, the amplitude of shear wave splitting reported in some regions of the oceanic mantle is large (~1 s) (e.g., Park & Levin 2002, Savage 1999), which is difficult to attribute to the olivine A-type fabric (assuming a thickness of 200 km). A complication in interpreting anisotropy in the asthenosphere is the

possible role of secondary convection. Secondary convection modifies the deformation geometry and hence the seismic anisotropy. Indeed Montagner (2002) invoked secondary convection to explain the band of weak anisotropy in the Pacific. Because secondary convection reduces the amplitude of azimuthal anisotropy, the presence of strong azimuthal anisotropy in the asthenosphere is good evidence of E-type fabric in the asthenosphere. Another difference between the olivine A- and E-type fabrics is the nature of asymmetry. The direction of the olivine [100] axes is not exactly parallel to the shear direction but has some finite tilt. The sense of this tilt is opposite between these two fabrics (see **Figure 3**). Consequently, if the tilt can be detected (e.g., Levin & Park 1998) and if the sense of shear in the asthenosphere can be inferred from other geophysical observations or geodynamic considerations, then one can distinguish olivine A-type fabric from E-type fabric.

Changes in anisotropic fabrics will cause seismic discontinuities if the transition is sharp. Some of the enigmatic discontinuities in the upper mantle might be caused by the transition in mineral fabrics (e.g., Deuss & Woodhouse 2004, Karato 1992).

The anisotropic fabric may also be detected from the anisotropy in electrical conductivity. According to the model by Karato (1990), electrical conductivity of olivine with some hydrogen is expected to be highly anisotropic. This was confirmed by the experimental study by Yoshino et al. (2006). Gatzemeier & Moorkamp (2005) and Simpson & Tommasi (2005) discussed the significance of anisotropy in electrical conductivity in relation to the role of hydrogen. However, the resolution for detecting conductivity anisotropy is less than that of seismic anisotropy.

The anisotropic structure of upwelling plumes (in the upper mantle) is likely complicated because of the combination of the change in flow geometry and in water content. If the plume materials contain several times more water than asthenosphere materials, the olivine LPO in the plume column is likely C-type: The olivine [001] axis is nearly vertical. However, because of the high water content and the higher temperatures, partial melting will likely start relatively deep in the upper mantle (∼100–150 km) (e.g., Hirschmann 2006). Upon partial melting, much of the water is removed from olivine (and other minerals) (Karato 1986). Consequently, olivine LPO changes from C-, to E-, and finally to A-type as dehydration proceeds. The resulting seismic anisotropy depends on the interplay between dehydration-induced change in LPO and the change in flow geometry as a plume hits the lithosphere. The depth at which melting causes dewatering depends on the geotherm and the water content of plume material. For a plausible range of water contents (∼0.01–0.05 wt%) and geotherm (an excess of 100–200 K above typical geotherm), a significant degree of partial melting and consequent dehydration likely occur at a depth of ∼100–200 km (compare this with ∼60 km for a typical mid-ocean ridge). This means that when a plume interacts with the asthenosphere (as, for example, in Hawaii), a large fraction of the (solid) materials supplied by plume to the asthenosphere will be water poor (water-rich melt will be removed to the surface without much interaction with the surrounding materials). If this is the case, the olivine LPO in the water-poor (shallow) asthenosphere will be A-type, as opposed to E-type (or C-type) predicted for typical (deep) asthenosphere, leading to an anomalously strong $V_{SH} > V_{SV}$ anisotropy. This model gives an explanation for the observed unique seismic anisotropy in the central

Pacific as reported by Ekström & Dziewonski (1998) and provides a new view of the plume-asthenosphere interaction in terms of water transport. Owing to the high temperature and high water content, asthenospheric materials after their interaction with a plume have less water than the asthenospheric materials in the normal regions.

Gaherty (2001) reported seismological observations on the structure of the plume root beneath Iceland. He reported evidence suggesting a transition from $V_{SH} > V_{SV}$ (in the shallow portions) to $V_{SV} > V_{SH}$ (in the deeper portions) at around 100 km, and interpreted these observations in terms of a change in flow geometry. However, the

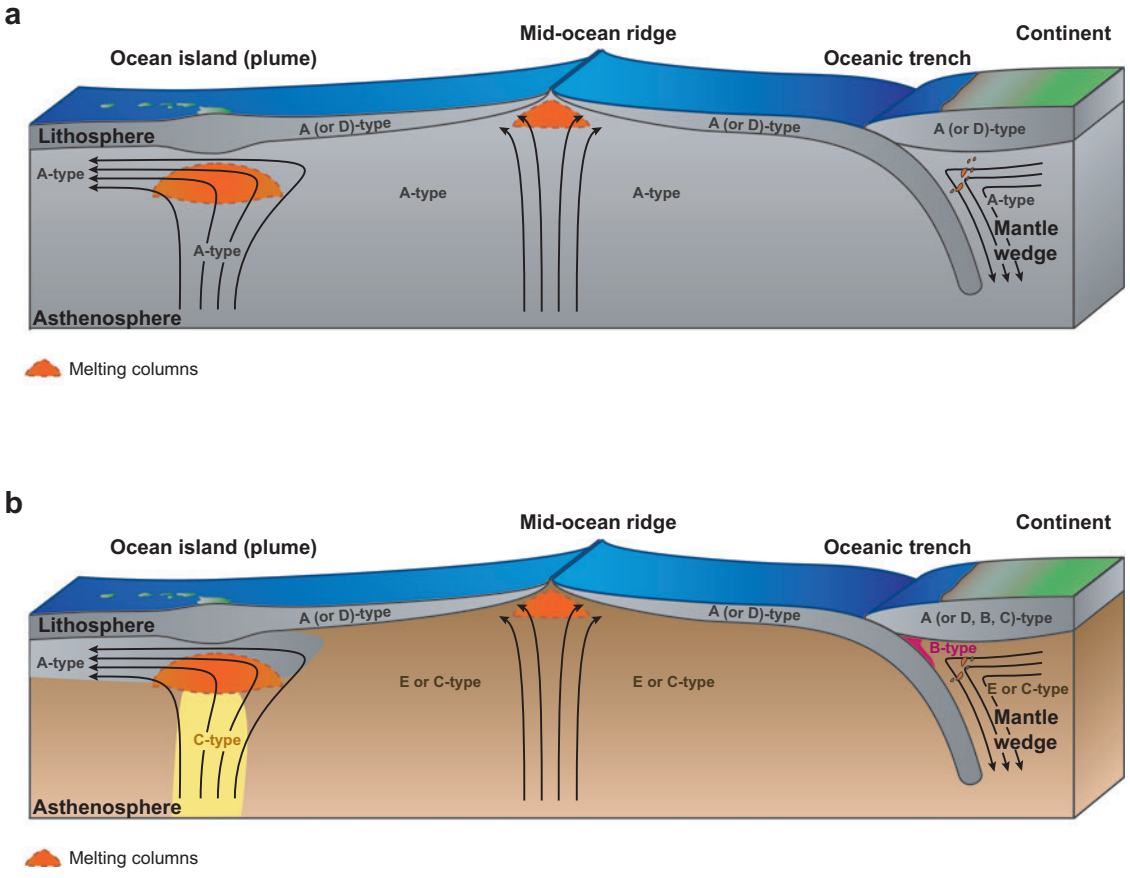

Figure 10

Diagrams illustrating the likely distribution of olivine fabrics in the upper mantle. The orange-shaded regions beneath the mid-ocean ridge and the plume, and within the subduction wedge, are the melting column where a significant amount of melting occurs. This column is deeper for plumes because of the higher temperature and larger water content. (*a*) In a conventional model of olivine LPO, LPO is A-type everywhere (except in some localized regions where high-stress deformation occurs where the D-type fabric will develop). (*b*) In the new model developed here, olivine LPO below the lithosphere has a rich variety reflecting the variation in water content, temperature, and stress.

same observations can also be interpreted in terms of a change in olivine fabrics due to dehydration at a depth of ~100 km (e.g., Karato 2003a). However, interpretation of seismic anisotropy of plume roots is complicated by the interplay between the changes in flow geometry and in olivine LPO. Detailed study of the anisotropic structures of a plume will provide us with an important clue as to the role of plumes to transport water into the upper mantle.

In **Figure 10**, the distribution of olivine LPO predicted from our laboratory studies is compared with the conventional model. In the conventional model, olivine LPO was considered to be A-type everywhere (except in local high-stress regions where the D-type fabric will develop). In contrast, our new model predicts a rich variety in olivine fabrics, particularly in the subduction zones and in regions where a plume interacts with the asthenosphere. Some of the enigmatic observations of seismic anisotropy may be attributed to local or regional variation in olivine LPO caused by the variation in deformation conditions.

SUMMARY POINTS

1. The seismic anisotropy of Earth's upper mantle can be explained by the LPO of anisotropic mineral such as olivine.
2. The relationship between the nature of seismic anisotropy and flow geometry in olivine depends on the physical/chemical conditions at which the LPO is formed.
3. The influence of water, stress, and temperature on olivine fabrics is large and is well documented by the experimental studies. Seismic anisotropy in the depleted regions (lithosphere) is due to the olivine A- (or D-)type fabric, as has been known in the past, but anisotropy in the undepleted regions (deep asthenosphere, plumes, subduction zones) is caused by other types of olivine fabrics (B-, C-, or E-type fabric), for which the relationship between anisotropy and flow geometry is different from that for the well-known A-type fabric.
4. The influence of partial melting is primarily through the redistribution of water, and the presence of melt does not have a direct effect on LPO.
5. These new results provide an explanation for enigmatic observations in subduction zones and in the central Pacific. Our interpretation of the strong shear wave polarization anomaly in the central Pacific suggests a new view of the role of plumes to transport water into the asthenosphere.

FUTURE ISSUES

1. Although there have been some arguments on the pressure effects on olivine LPO, the influence of pressure on olivine (and other mineral) LPO has

not been investigated in any detail. Previous studies were on samples with large water content or at high stress levels. Both of these factors promote deformation with **b** = [001] slip systems and hence do not demonstrate intrinsic pressure effects. New experiments need to be conducted at low stress and low water content conditions for a broad range of pressures to explore intrinsic effects of pressure.

2. The physical/chemical conditions for some fabric boundaries such as A-E and E-C boundaries are critical for understanding the distribution of water in the asthenosphere and plumes from seismic anisotropy. However, much of the existing data on these boundaries are at high stress levels. The morphology of these boundaries likely changes at low stress levels, where different forms of flow law would apply. Also, different processes such as grain-boundary migration may contribute to LPO under these conditions. Additional data at lower stress levels and at various temperatures are needed to address these issues.
3. The currently available experimental data on LPO evolution in olivine are mostly for a constant deformation geometry. In many geological settings, deformation geometry of a given material changes with time (e.g., beneath a mid-ocean ridge or a plume). The process by which a material will adjust its LPO with evolving deformation geometry needs to be investigated.
4. Most of the existing experimental data on LPO are for olivine. Similar studies need to be carried out on other minerals (particularly orthopyroxene) that constitute a significant fraction of the upper mantle. In addition, fabric developments in a multiphase mixture might be different from those in a single-phase material. Experiments on a multiphase mixture will be useful to address this issue.
5. The LPO of naturally deformed peridotites need to be investigated for a broad range of samples, with close attention paid to the correlation between fabrics and the chemical and physical conditions of deformation. The focus should be on samples from deep upper mantle (asthenosphere, plumes, and deep continental roots).
6. The anisotropic structures of plume roots and the deep upper mantle need to be investigated in detail from a seismological perspective. The anisotropic structures in these regions contain a clue as to the way in which water is distributed in Earth's upper mantle.

DISCLOSURE STATEMENT

The authors are not aware of any biases that might be perceived as affecting the objectivity of this review.

ACKNOWLEDGMENTS

This study is supported partially by NSF (SK), University of Minnesota (HJ), and JSPS (IK). We have benefited from helpful discussions with Erik Kneller, Maureen Long, Jun-ichi Nakajima, Jeffery Park, Andrea Tommasi, and Peter van Keken. Akira Hasegawa provided us with an unpublished dataset of GPS measurements in Tohoku, Japan. Jeffery Park and Paul Raterron are thanked for sending us their papers prior to publication.

LITERATURE CITED

Avé Lallemant HG. 1967. Structural and petrological analysis of an 'Alpine-type' peridotite. The lherzolite of the French Pyrenees. *Leidse Geol. Meded.* 42:1–57

Avé Lallemant HG, Carter NL. 1970. Syntectonic recrystallization of olivine and modes of flow in the upper mantle. *Geol. Soc. Am. Bull.* 81:2203–20

Bai Q, Mackwell SJ, Kohlstedt DL. 1991. High temperature creep of olivine single crystals. 1. Mechanical results for buffered samples. *J. Geophys. Res.* 96:2441–63

Becker TW, Kellogg JB, O'Connell RJ. 2003. Comparison of azimuthal seismic anisotropy from surface waves and finite strain from global mantle-circulation models. *Geophys. J. Int.* 155:696–714

Bell DR, Rossman GR, Maldener J, Endisch D, Rauch F. 2003. Hydroxide in olivine: a quantitative determination of the absolute amount and calibration of the IR spectrum. *J. Geophys. Res.* 108:10.1029/2001JB000679

Ben Ismail W, Mainprice D. 1998. An olivine fabric database: an overview of upper mantle fabrics and seismic anisotropy. *Tectonophysics* 296:145–57

Buiskool Toxopeus JMA. 1976. Petrofabrics, microstructures and dislocation substructures of olivine in a peridotite mylonite (Alpe Arami, Switzerland). *Leidse Geol. Meded.* 51:1–36

Buttles J, Olson P. 1998. A laboratory model of subduction zone anisotropy. *Earth Planet. Sci. Lett.* 164:245–62

Bystricky M, Kunze K, Burlini L, Burg J-P. 2001. High shear strain of olivine aggregates: rheological and seismic consequences. *Science* 290:1564–67

Carter NL, Avé Lallemant HG. 1970. High temperature deformation of dunite and peridotite. *Geol. Soc. Am. Bull.* 81:2181–202

A detailed analysis of dominant slip systems under various conditions is presented.

Carter NL, Baker DW, George RP Jr. 1972. Seismic anisotropy, flow, and constitution of the upper mantle. In *Flow and Fracture of Rocks*, ed. HC Heard, IY Borg, NL Carter, CB Raleyigh, pp. 167–90. Washington. DC: Am. Geophys. Union

Christensen NI, Lundquist SM. 1982. Pyroxene orientations within the upper mantle. *Geol. Soc. Am. Bull.* 93:279–88

Couvy H, Frost DJ, Heidelbach F, Nyilas K, Ungar T, et al. 2004. Shear deformation experiments of forsterite at 11 GPa-1400°C in the multianvil apparatus. *Eur. J. Mineral.* 16:877–89

Debayle E, Kennett BLN, Priestley K. 2005. Global azimuthal seismic anisotropy and the unique plate-motion deformation of Australia. *Nature* 433:509–12

Deuss A, Woodhouse JH. 2004. The nature of the Lehmann discontinuity from its seismological Clapeyron slope. *Earth Planet. Sci. Lett.* 225:295–304

Dobrzhinetskaya L, Green HW II, Wang S. 1996. Alpe Arami: a peridotite massif from depths of more than 300 kilometers. *Science* 271:1841–45

Drury MR. 1991. Hydration-induced climb dissociation of dislocations in naturally deformed mantle olivine. *Phys. Chem. Miner.* 18:106–16

Durinck J, Legris A, Cordier P. 2005. Pressure sensitivity of olivine slip systems: first-principle calculations of generalised stacking faults. *Phys. Chem. Miner.* 32:646–54

Ekström G, Dziewonski AM. 1998. The unique anisotropy of the Pacific upper mantle. *Nature* 394:168–72

Frese K, Trommsdorff V, Kunze K. 2003. Olivine [100] normal to foliation: lattice preferred orientation in prograde garnet peridotite formed at high H_2O activity, Cima di Ganone (Central Alps). *Contrib. Mineral. Petrol.* 145:75–86

Gaherty JB. 2001. Seismic evidence for hotspot-induced buoyant flow beneath the Reykjanes ridge. *Science* 293:1645–47

Gatzemeier A, Moorkamp M. 2005. 3D modelling of electrical anisotropy from electromagnetic array data: hypothesis testing for different upper mantle conduction mechanisms. *Phys. Earth Planet. Inter.* 149:225–42

George RP Jr. 1975. *The Internal Structure of the Troodos Ultramafic Complex, Cyprus*. Stony Brook: SUNY Press

Gleason GC, Tullis J. 1993. Improving flow laws and piezometers for quartz and feldspar aggregates. *Geophys. Res. Lett.* 20:2111–14

Goetze C. 1978. The mechanisms of creep in olivine. *Philos. Trans. R. Soc. London A* 288:99–119

An insightful review of classical works on olivine deformation.

Haggerty SE, Sautter V. 1990. Ultra deep (>300 km) ultramafic, upper mantle xenoliths. *Science* 248:993–96

Heggie M, Jones R. 1986. Models of hydrolytic weakening in quartz. *Philos. Mag. A* 53:L65–L70

Hirschmann MM. 2006. Water, melting, and the deep Earth H_2O cycle. *Annu. Rev. Earth Planet. Sci.* 34:629–53

Holtzman BK, Kohlstedt DL, Zimmerman ME, Heidelbach F, Hiraga K, Hustoft J. 2003. Melt segregation and strain partitioning: implications for seismic anisotropy and mantle flow. *Science* 301:1227–30

Huang X, Xu Y, Karato S. 2005. Water content of the mantle transition zone from the electrical conductivity of wadsleyite and ringwoodite. *Nature* 434:746–49

Jin D. 1995. *Deformation microstructures of some ultramafic rocks*. MSc thesis. Univ. Minnesota, Minneapolis. 115 pp.

Jung H, Karato S. 2001. Water-induced fabric transitions in olivine. *Science* 293:1460–63

The first report on the water-induced fabric transitions demonstrated by simple shear, large-strain deformation experiments for a broad range of water content.

Jung H, Katayama I, Jiang Z, Hiraga T, Karato S. 2006. Effects of water and stress on the lattice preferred orientation in olivine. *Tectonophysics* 421:1–22

Kaminski E. 2002. The influence of water on the development of lattice preferred orientation in olivine aggregates. *Geophys. Res. Lett.* 29:17-1–4, doi: 10.1029/2002GL014710

Karato S. 1986. Does partial melting reduce the creep strength of the upper mantle? *Nature* 319:309–10

Karato S. 1990. The role of hydrogen in the electrical conductivity of the upper mantle. *Nature* 347:272–73

Karato S. 1992. On the Lehmann discontinuity. *Geophys. Res. Lett.* 19:2255–58
Karato S. 1995. Effects of water on seismic wave velocities in the upper mantle. *Proc. Jpn. Acad.* 71:61–66
Karato S. 1998. Seismic anisotropy in the deep mantle, boundary layers and geometry of mantle convection. *Pure Appl. Geophys.* 151:565–87
Karato S. 2003a. *Dynamic Structure of the Deep Earth: An Interdisciplinary Approach*. Princeton, NJ: Princeton Univ. Press. 241 pp.
Karato S. 2003b. Mapping water content in Earth's upper mantle. In *Inside the Subduction Factory*, ed. JE Eiler, pp. 135–52. Washington, DC: AGU
Karato S. 2006. Influence of hydrogen-related defects on the electrical conductivity and plastic deformation of mantle minerals: a critical review. In *Earth's Deep Water Cycle*, ed. SD Jacobsen, S van der Lee, pp. 113–29. Washington, DC: AGU
Karato S. 2008. *Deformation of Earth Materials: Introduction to the Rheology of the Solid Earth*. Cambridge, UK: Cambridge Univ. Press. 462 pp.
Karato S, Jung H. 2003. Effects of pressure on high-temperature dislocation creep in olivine polycrystals. *Philos. Mag. A* 83:401–14
Karato S, Lee K-H. 1999. Stress-strain distribution in deformed olivine aggregates: inference from microstructural observations and implications for texture development. Int. Conf. Textures Mater., 12th, ed. JA Szpunar, pp. 1546–55. Montreal: Textures Mater.
Karato S, Paterson MS, Fitz Gerald JD. 1986. Rheology of synthetic olivine aggregates: influence of grain-size and water. *J. Geophys. Res.* 91:8151–76
Karato S, Rubie DC. 1997. Toward experimental study of plastic deformation under deep mantle conditions: a new multianvil sample assembly for deformation experiments under high pressures and temperatures. *J. Geophys. Res.* 102:20111–22
Katayama I, Jung H, Karato S. 2004. New type of olivine fabric at modest water content and low stress. *Geology* 32:1045–48
Katayama I, Karato S. 2006. Effects of temperature on the B- to C-type fabric transition in olivine. *Phys. Earth Planet. Inter.* 157:33–45
Katayama I, Karato S, Brandon M. 2005. Evidence of high water content in the deep upper mantle inferred from deformation microstructures. *Geology* 33:613–16
Kneller EA, van Keken PE, Karato S, Park J. 2005. B-type olivine fabric in the mantle wedge: insights from high-resolution non-Newtonian subduction zone models. *Earth Planet. Sci. Lett.* 237:781–97
Kneller EA, van Keken PE, Katayama I, Karato S. 2007. Stress, strain, and B-type olivine fabric in the fore-arc mantle: sensitivity tests using high-resolution steady-state subduction zone models. *J. Geophys. Res.* 112:10.1029/2006JB004544
Kohlstedt DL. 2006. The role of water in high-temperature rock deformation. In *Water in Nominally Anhydrous Minerals*, ed. H Keppler, JR Smyth, pp. 377–96. Washington, DC: MSA
Kohlstedt DL, Keppler H, Rubie DC. 1996. Solubility of water in the α, β and γ phases of $(Mg,Fe)_2SiO_4$. *Contrib. Mineral. Petrol.* 123:345–57
Levin V, Park J. 1998. P-SH conversions in layered media with hexagonal symmetric anisotropy: a cook book. *Pure Appl. Geophys.* 151:669–97

Long MD, van der Hilst RD. 2005. Upper mantle anisotropy beneath Japan from shear wave splitting. *Phys. Earth Planet. Inter.* 151:206–22

Mackwell SJ, Kohlstedt DL, Paterson MS. 1985. The role of water in the deformation of olivine single crystals. *J. Geophys. Res.* 90:11319–33

Mainprice D, Barroul G, Ben Ismail W. 2000. The seismic anisotropy of the Earth's mantle: from single crystal to polycrystal. In *Earth's Deep Interior*, ed. S-I Karato, A Forte, RC Liebermann, G Masters, L Stixrude, pp. 237–64. Washington, DC: AGU

Mainprice D, Tommasi A, Couvy H, Cordier P, Frost DJ. 2005. Pressure sensitivity of olivine slip systems and seismic anisotropy of Earth's upper mantle. *Nature* 433:731–33

Mehl L, Hacker BR, Hirth G. 2003. Arc-parallel flow within the mantle wedge: evidence from the accreted Talkeetna Arc, south central Alaska. *J. Geophys. Res.* 108:10.1029/2002JB002233

Mei S, Kohlstedt DL. 2000. Influence of water on plastic deformation of olivine aggregates. 2. Dislocation creep regime. *J. Geophys. Res.* 105:21471–81

Mercier J-CC.1985. Olivine and pyroxenes. In *Preferred Orientation in Deformed Metals and Rocks: Introduction to Modern Texture Analysis*, ed. H-R Wenk, pp. 407–33. Orlando, FL: Academic

Mizukami T, Wallis SR, Yamamoto J. 2004. Natural examples of olivine lattice preferred orientation patterns with a flow-normal a-axis maximum. *Nature* 427:432–36

Möckel JR. 1969. Structural petrology of the garnet-peridotite of Alpe Arami (Ticino, Switzerland). *Leidse Geol. Meded.* 42:61–130

Montagner J-P. 2002. Upper mantle low anisotropy channels below the Pacific Plate. *Earth Planet. Sci. Lett.* 202:263–74

Montagner J-P, Guillot L. 2002. Seismic anisotropy and global geodynamics. In *Plastic Deformation of Minerals and Rocks*, ed. S Karato, H-R Wenk, pp. 353–85. Washington, DC: MSA

Montagner J-P, Tanimoto T. 1990. Global anisotropy in the upper mantle inferred from the regionalization of phase velocities. *J. Geophys. Res.* 95:4797–819

Montagner J-P, Tanimoto T. 1991. Global upper mantle tomography of seismic wave velocities and anisotropies. *J. Geophys. Res.* 96:20337–51

Nabarro FRN. 1967. *Theory of Crystal Dislocations*. Oxford, UK: Oxford Univ. Press

Nakajima J, Hasegawa A. 2004. Shear-wave polarization anisotropy and subduction-induced flow in the mantle wedge of northern Japan. *Earth Planet. Sci. Lett.* 225:365–77

Nicolas A. 1993. Why fast polarization direction of SKS seismic waves are parallel to mountain belts. *Phys. Earth Planet. Inter.* 78:337–42

Nicolas A, Bouchez JL, Boudier F, Mercier J-CC. 1971. Textures, structures and fabrics due to solid state flow in some European lherzolites. *Tectonophyiscs* 12:55–86

Nicolas A, Boudier F, Boullier AM. 1973. Mechanisms of flow in naturally and experimentally deformed peridotites. *Am. J. Sci.* 273:853–76

Marked anisotropy in the weakening effect of olivine by water, as shown in their figures 8, 9, and 10, formed a basis for the hypothesis of water-induced fabric transitions by Karato (1995).

A report on unusual olivine fabric (B-type LPO).

Using global inversion of surface wave data, the authors determined both polarization and azimuthal anisotropy and detected the depth and regional variation in anisotropy.

A clear demonstration of trench-parallel to trench-normal transition in the direction of the faster shear wave polarization in the subduction zone of Tohoku (northeastern) Japan.

A classic paper on the deformation fabrics of peridotites and their implications for seismic anisotropy.

Nicolas A, Christensen NI. 1987. Formation of anisotropy in upper mantle peridotite: a review. In *Composition, Structure and Dynamics of the Lithosphere-Asthenosphere System*, ed. K Fuchs, C Froidevaux, pp. 111–23. Washington, DC: AGU

Nishihara Y, Shinmei T, Karato S. 2006. Grain-growth kinetics in wadsleyite: effects of chemical environment. *Phys. Earth Planet. Inter.* 154:30–43

Park J, Levin V. 2002. Seismic anisotropy: tracing plate dynamics in the mantle. *Science* 296:485–89

Paterson MS. 1982. The determination of hydroxyl by infrared absorption in quartz, silicate glass and similar materials. *Bull. Mineral.* 105:20–29

Peierls R. 1940. The size of a dislocation. *Proc. Phys. Soc.* 52:34–37

Phakey P, Dollinger G, Christie J. 1972. Transmission electron microscopy of experimentally deformed olivine crystals. In *Flow and Fracture of Rocks*, ed. HC Heard, IY Borg, NL Carter, CB Raleigh, pp. 117–38. Washington, DC: AGU

Poirier J-P. 1985. *Creep of Crystals*. Cambridge, UK: Cambridge Univ. Press. 260 pp.

Raterron P, Chen J, Li L, Weidner DJ, Cordier P. 2007. Pressure-induced slip system transition in forsterite: single-crystal rheological properties at mantle pressure and temperature. *Am. Mineral.* 92:1436–45

Ringwood AE. 1975. *Composition and Structure of the Earth's Mantle*. New York: McGraw-Hill. 618 pp.

Ross JV, Nielsen KC. 1978. High-temperature flow of wet polycrystalline enstatite. *Tectonophysics* 44:233–61

Russo R, Silver PG. 1994. Trench-parallel flow beneath the Nazca plate from seismic anisotropy. *Science* 263:1105–11

Savage MK. 1999. Seismic anisotropy and mantle deformation: What have we learned from shear wave splitting? *Rev. Geophys.* 37:65–106

Sawaguchi T. 2004. Deformation history and exhumation process of the Horoman Peridotite Complex, Hokkaido, Japan. *Tectonophysics* 379:109–26

Shito A, Karato S, Matsukage KN, Nishihara Y. 2006. Toward mapping water content, temperature and major element chemistry in Earth's upper mantle from seismic tomography. In *Earth's Deep Water Cycle*, ed. SD Jacobsen, S van der Lee, pp. 225–36. Washington, DC: AGU

Simpson F, Tommasi A. 2005. Hydrogen diffusivity and electrical anisotropy of a peridotite mantle. *Geophys. J. Int.* 160:1092–102

Skemer PA, Katayama I, Karato S. 2006. Deformation fabrics of a peridotite from Cima di Gagnone, central Alps, Switzerland: evidence of deformation under water-rich condition at low temperatures. *Contrib. Mineral. Petrol.* 152:43–51

Smith GP, Wiens DA, Fischer KM, Dorman LM, Hildebrand JA. 2001. A complex pattern of mantle flow in the Lau back-arc. *Science* 292:713–16

Tommasi A. 1998. Forward modeling of the development of seismic anisotropy in the upper mantle. *Earth Planet. Sci. Lett.* 160:1–13

Wang D, Mookherjee M, Xu Y, Karato S. 2006. The effect of water on the electrical conductivity in olivine. *Nature* 443:977–80

Wenk H-R. 1985. *Preferred Orientation in Deformed Metals and Rocks: An Introduction to Modern Texture Analysis*. Orlando, FL: Academic. 610 pp.

Xu Z, Wang Q, Ji S, Chen J, Zeng L, et al. 2006. Petrofabric and seismic properties of garnet peridotite from the UHP Sulu terrane (China): implications for olivine deformation mechanism in a cold dry subducting continental slab. *Tectonophysics* 421:111–27

Yan H. 1992. *Dislocation recovery in olivine*. MS thesis. Univ. Minn., Minneapolis. 93 pp.

Yoshino G. 1961. Structural-petrological studies of peridotite and associated rocks of the Higashi-Akaishi-Yama district, Shikoku, Japan. *J. Sci. Hiroshima Univ. Ser.* C3:343–402

Yoshino T, Matsuzaki T, Yamashita S, Katsura T. 2006. Hydrous olivine unable to account for conductivity anomaly at the top of the asthenosphere. *Nature* 443:974–76

Zhang S, Karato S. 1995. Lattice preferred orientation of olivine aggregates deformed in simple shear. *Nature* 375:774–77

Zhang S, Karato S, Fitz Gerald J, Faul UH, Zhou Y. 2000. Simple shear deformation of olivine aggregates. *Tectonophysics* 316:133–52

Zimmerman MR, Zhang S, Kohlstedt DL, Karato S. 1999. Melt distribution in mantle rocks deformed in shear. *Geophys. Res. Lett.* 26:1505–8

RELATED RESOURCES

Maupin V, Park J. 2008. Seismic anisotropy: theory and observations. In *Treatise in Geophysics*, ed. B Romanowicz, AM Dziewonski, Vol. 1, pp. 289–321. Amsterdam: Elsevier

Annual Review
of Earth and
Planetary Sciences
Volume 36, 2008

Contents

Indexes

Errata

An online log of corrections to *Annual Review of Earth and Planetary Sciences* articles may be found at http://earth.annualreviews.org